Petrogenesis of Liucn Pluton in the Eastern Section of Jiangnan Orogenic belt，China: Zircon U-Pb Age, Petrogeochemistry and Sr-Nd -Hf Isotope Characters

Fang Chen *, Jianguo Du , Jingjing Chen , Mingming Sun

Posted Date: 13 November 2024

doi: 10.20944/preprints202411.0865.v1

Keywords: Liucun pluton; petrogeochemistry; petrogenesis; pircon U-Pb age; Sr-Nd -Hf isotope; eastern section of Jiangnan orogenic belt

Article

Petrogenesis of Liucn Pluton in the Eastern Section of Jiangnan Orogenic Belt, China: Zircon U-Pb Age, Petrogeochemistry and Sr-Nd-Hf Isotope Characters

Fang Chen [1,2,3,*], Jianguo Du [1,2,3], Jingjing Chen [1] and Mingming Sun [1]

[1] Geological Survey of Anhui Province (Anhui Institute of Geological Sciences), Hefei 230001, China
[2] Technology Innovation Center of Coverage Area Deep Resource Exploration Engineering, MNR, Hefei 230001, China
[3] Engineering Research Center of Deep Resource Exploration of Anhui Province, Hefei 230001, China
* Correspondence: chenfang0929@163.com

Abstract: The Liucun pluton locates in the area that adjoin to Zhejiang province in the eastern section of the Jiangnan orogenic belt. It is mainly composed of monzonitic granite and granites, with late intrusion of syenite-granite. Numerous deposits (points) were found on the southwest side of the pluton. The characteristics of major elements show that the Liucun rock masses are all silica-rich, potassium-rich and peraluminous high potassium calc-alkaline rocks with right-leaning characteristics of light rare earth element enrichment and heavy rare earth element deficit. The degree of differentiation of light and heavy rare earth elements is similar, with obvious negative Eu anomaly. Zircon LA-ICP-MS U-Pb weighted mean ages of monzonitic granite, porphyritic biotite monzonitic granite and granite are 130.50±0.55Ma, 128.95±0.46Ma and 133.8±1.0Ma, which belong to the late stage of magmatic activity in the Jiangnan uplift belt. The emplacement time of granite is slightly earlier than that of monzonitic granite. The characteristics of major, trace and rare earth elements in Liucun pluton are typical of A-type granites, and the characteristics of major, trace elements and Hf isotopes indicate the shell-source characteristics of Liucun pluton. From the perspective of the whole Jiangnan orogenic belt in southern Anhui, the value of the late stage rock $(^{87}Sr/^{86}Sr)_i$, including the Liucun pluton, is smaller than that of the early stage, and the $\varepsilon_{Nd}(t)$ and $\varepsilon_{Hf}(t)$ values of the late stage rock are larger than that of the early stage, and the distribution range is narrower than that of the early stage, which indicates that the late stage rock is mixed with a greater proportion of new mantle materials than that of the early granitic rock. The Liucun pluton is derived from the secondary partial melting of the ancient lower crust in Mesoproterozoic, and during the melting process, more new mantle source materials were mixed in due to the transformation of tectonic environment. The formation of the main body of Liucun pluton (monzonitic granite) may be influenced by extrusion collision, and the Liucun pluton was formed in the intraplate stretching environment after the Late Jurassic-Early Cretaceous tectonic transition period.

Keywords: Liucun pluton; petrogeochemistry; petrogenesis; Zircon U-Pb age; Sr-Nd-Hf isotope; Eastern section of Jiangnan orogenic belt

1. Introduction

The late Mesozoic granitoid intrusive rocks are widely distributed in the eastern section of Jiangnan Orogenic belt, which can appear alone or many of them are produced as composite rocks, and are unique in the late Mesozoic magmatic rock belt of the eastern continental margin of China. According to the geological history of Anhui Province, it is named as the southern Anhui magmatic belt of the Lower Yangtze tectonic magmatic belt [1,2]. Its distribution is bounded by the Zhouwang fault. The Yanshanian monzoniite-syenite-dominated acid intrusive rocks are mainly developed in

 doi:10.20944/preprints202411.0865.v1

the south of the fault, and the basaltic (secondary) volcanic rocks are mainly developed in the north of the fault. The main fault structures are near EW, NE, NW, etc. (Figure 1). Based on the formation of Neoproterozoic collision orogeny and metamorphic basement, the magmatic belt was formed through multi-stage tectonic evolution such as early Paleozoic fold uplift and Mesozoic intracontinental tectonics [2–7], especially the Yanshanian metallogenic explosion in eastern China triggered strong magmatic activity and mineralization, and the region was rich in copper, tungsten, molybdenum, gold, silver, lead, zinc, uranium and other minerals [8,9]. In recent years, a series of large or super-large W-Mo-Cu-Au deposits have been discovered in the Jiangnan uplift belt [1,10–14], which makes the study of magmatic rocks in the zone attract more and more attention from the geological community.

However, few studies have been done on the Liucun pluton, which is located in the eastern part of Jiangnan Orogenic belt, adjacent to Anhui and Zhejiang provinces. Previous studies have only been done on the diagenetic age and petrogeochemistry of the monzonitic granites in the pluton [15,16], however, there are some shortcomings in the studies of Sr-Nd isotope characteristics of whole rock, Lu-Hf isotope characteristics of zircon, petrogenesis, diagenetic source area and tectonic environment.

Therefore, this paper takes Liucun pluton as the research object. Based on field investigation, the whole rock geochemistry, Sr-Nd isotope age, LA-ICPMS zircon U-Pb isotope age and in situ Lu-Hf isotope geochemistry of zircon are carried out, in an attempt to define its diagenesis age, petrogenesis, diagenesis source area and tectonic environment. The geochronological framework and petrogenesis of magmatic rocks in the Jiangnan orogenic belt are supplemented and enriched, thus providing important basic geological data for further study of the late Mesozoic tectonic evolution and mineralization of the Jiangnan orogenic belt.

2. Geological Survey and Samples

The neighboring area of Anhui and Zhejiang in the eastern section of Jiangnan Orogenic belt is located in the southeast of the Yangtze Plate. It has experienced the Jinning, Caledonian, Hercynian, Indosinian, Yanshan and Himalayan tectonic movements successively. The sedimentary characteristics, magmatic activity, metamorphism and mineralization of different tectonic movements have their own characteristics, which formed the present tectonic pattern. To the northwest are the Tanlu fault belt, Qinling Dabie Orogenic belt, North China plate and Middle Yangtze block; to the south are the Jiangnan Orogenic belt and the Cathaysian block, with a wedge-shaped structural geometry that is narrow in the west and wide in the east (Figure 1a). The division of tectonic units is bounded by the Gaotan fault zone (F5), the Lower Yangtze foreland zone (Lower Yangtze offset transition zone) in the north, and the Jiangnan uplift zone in the south. The stratigraphic division is bounded by the Jiangnan Fault zone (F2), with the Lower Yangtze stratigraphic zone to the north and Jiangnan stratigraphic zone to the south [17–19] (Figure 1b).

There are mesoproterozoic to early Paleozoic strata in the area, which can be divided into basement and cover strata. The basement is composed of middle and late proterozoic shallow metamorphic rocks, which are mainly slate, phyllite, metamorphic siltstone, metamorphic sandstone and medium-acid volcanic rocks, distributed in the southern region. The cap layer is composed of three major cap layers since Nanhua Period, which are Nanhua to early Silurian, late Carboniferous to early Triassic and late Triassic to Cretaceous, mainly distributed in the north and near Huangshan City. There are angular unconformity contacts between basement and cover layer and between cover layer [18].

Preprints.org (www.preprints.org) | NOT PEER-REVIEWED | Posted: 13 November 2024 doi:10.20944/preprints202411.0865.v1

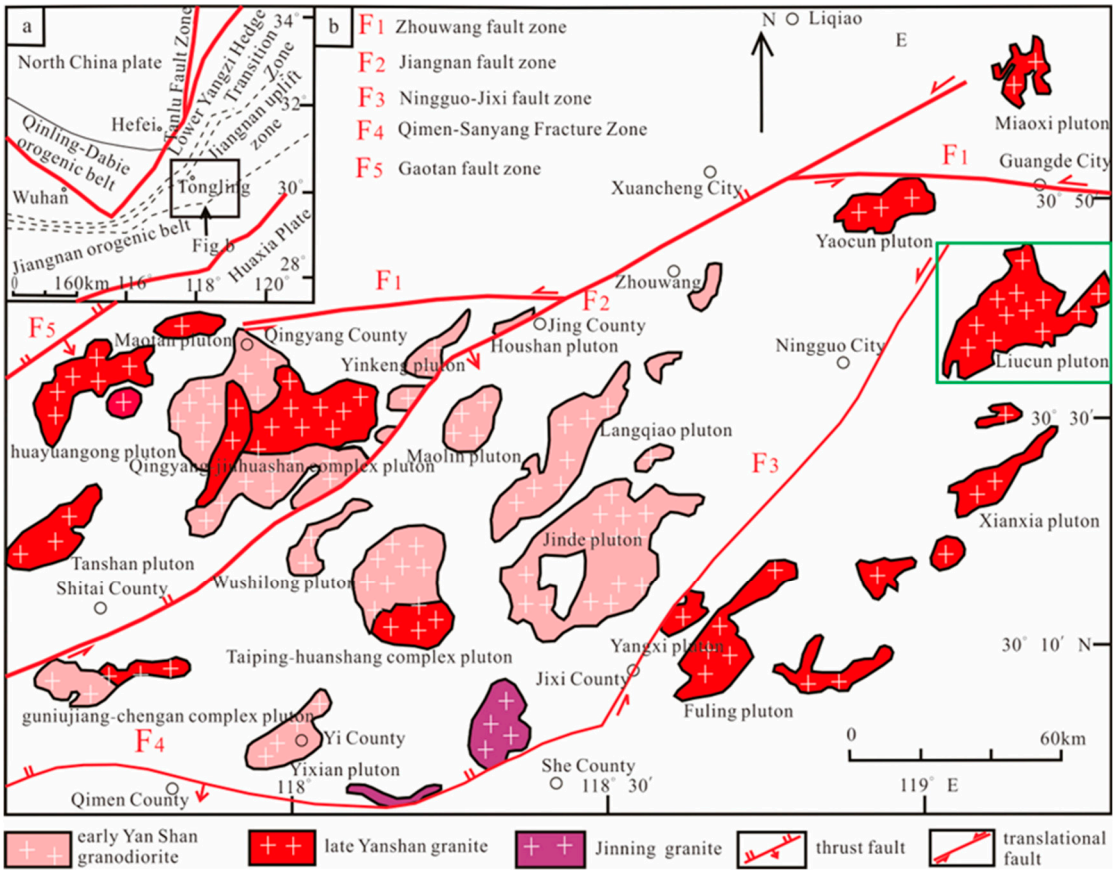

Figure 1. Map of location and magmatic rock distribution for the study area. a. Tectonic location map of the eastern section of Jiangnan orogenic belt; b. Sketch map of magmatic rock distribution in the eastern section of Jiangnan orogenic belt (after the paper [19]).

Fault structures developed in the region, mainly Mesozoic NNE-NE trending faults, and controlled the output of major granites and various minerals in the region [20,21].

The magmatic activity in the region is very strong, and the ultrabasic and acidic rocks are distributed. It mainly developed in Jinning stage and Yanshanian stage. In the early Neoproterozoic period (830～820Ma), the granodiorites of Xiuning, Shexian and Xucun are mainly found near Huangshan City. The late stage (780～760Ma) is the Lingshan, Lianhuashan and Shiershan granitic (porphyry) plutons [22,23]; The Mesozoic (150～120Ma) consists of granodiorite plutons such as Jingde, Langqiao and Taiping, granodiorite plutons such as Huangshan, Fuling, Liucun, Yaocun and Miaoxi in Yanshanian, and dozens of small rock strains [24,25] (Figure 1b).

The exposed area of the Liucun pluton is 213.14km^2, which is generally elliptic in the northeast direction and is obviously controlled by the structure. The pluton intrudes into the lower Silurian sand mudstone along the anticlinal axis composed of Cambrian strata, and is batholiplike, paraaxial and outward sloping. The boundary of pluton surrounding rock is clear, the contact surface is mostly outward dip, the dip angle is 40°～ 80°, and the northern part of pluton is inward. At the edge of the pluton, sometimes the trap body of angular sandstone can be seen, and the fine-grained (porphyritic) monzonitic granite (condensing edge) with a width ranging from tens of centimeters to hundreds of meters can be developed in local areas. The surrounding rock has silicification, hornification and other alteration, the alteration bandwidth ranges from 1000 to 2500m, and it contains iron and copper quartz veins, crystal and fluorite veins [16].

The main exposed strata around the pluton, from old to new, include the Cambrian Hetang Formation ($\in_1 h$), Cambrian to Ordovician Xiyangshan Formation ($\in_3 O_1 x$), Ordovician Yinzhubu Formation and Ningguo Formation union ($O_1 y$-n), Silurian Anji Formation ($S_1 a$) and Baidi Formation ($S_1 d$), Devonian Tangjiawu Formation ($D_{1\text{-}2} tn$), Cretaceous Pukou Formation ($K_{1\text{-}2} p$)), Quaternary (Q). Hetang Formation consists of black thin layer of carbonaceous, siliceous shale and mudstone with

 doi:10.20944/preprints202411.0865.v1

limestone lens. The Xiyangshan Formation is composed of rhythmical layers of gray-dark gray marl, nodular limestone or reticulate limestone. The interformation of Yinzhubu Formation and Ningguo Formation is calcareous mudstone with bluish gray and gray-green color. Anji Formation consists of gray-green, yellow-green fine sandstone, siltstone and sandy mudstone. The Dabaidi Formation consists of gray-green fine sandstone, siltstone with silty mudstone. Tangjiawu Formation is purplish red and gray-green quartz sandstone. The Pukou Formation consists of purple conglomerate, sand conglomerate and sandstone. The quaternary consists of clay, sand and gravel.

The rock types of Liucun pluton are mainly medium-fine grained porphyritic monzonitic granite, and some are medium-coarse grained monzonitic granite. The pluton is invaded by late fine grained syenite with nodules, branches and dike. A large number of deposits (points) have been found around the Liucun pluton, such as Guangde tungsten copper deposit in the middle of the pluton, Qiaotou Xiqiling tungsten ore in Ningguo City, Dali copper lead-zinc ore in Ningguo City and Lujiashan tungsten beryllium ore in Ningguo City in the southwest edge of the rock mass and its contact zone (Figure 2).

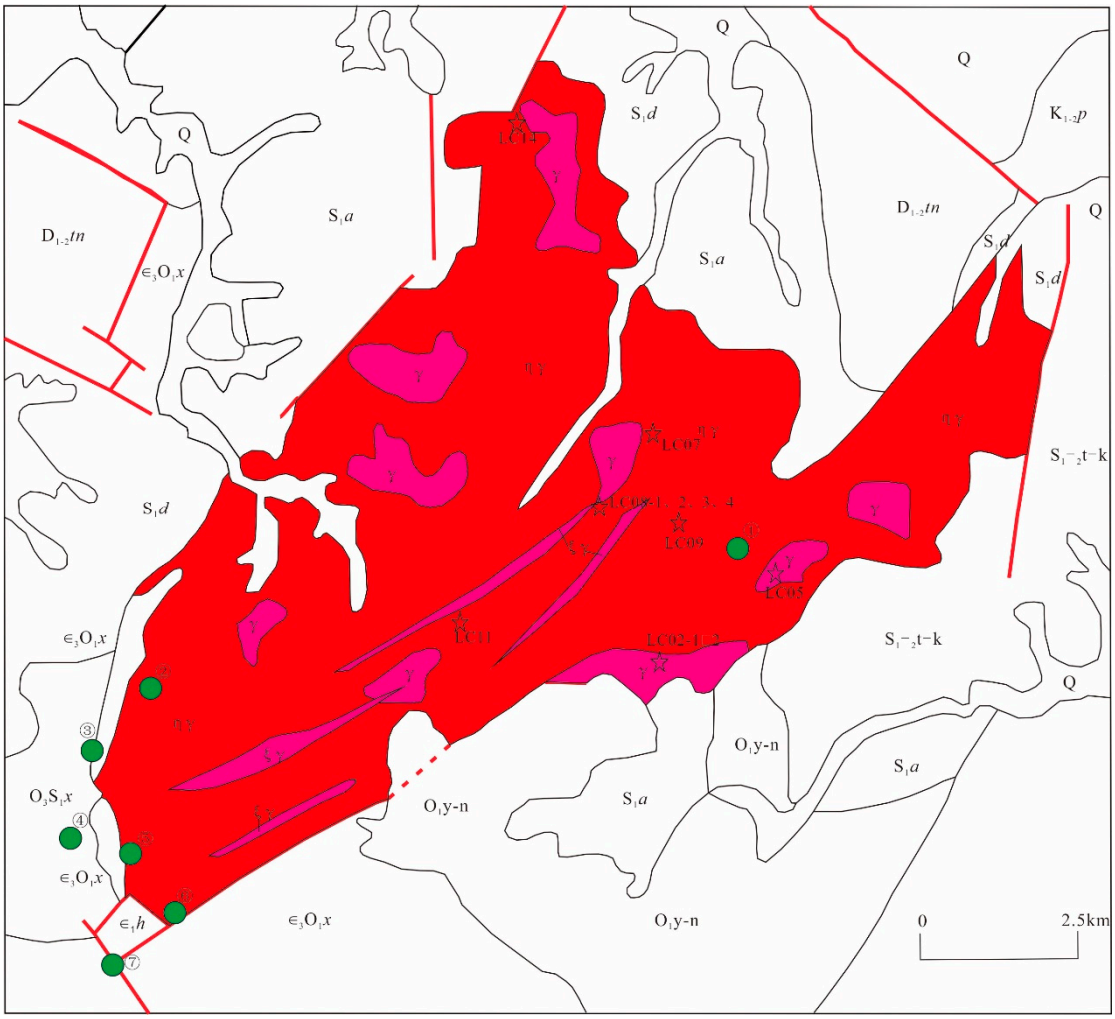

Figure 2. Geological sketch map of Liucun pluton Q— Quaternary; K1-2p—midddle-lower Cretaceous Pukou Formation; D1-2*tn*—middle –lower Devonian Tangjiawu Formation; S1*d*—lower Silurian Dabaidi Formation; S1*a*—low Silurian Anji Formation; O1*y-n*—lower Ordovician Yinzhubu Formation and Ningguo Formation; ∈ 3 O 1 *x*—upper Cambrian-lower Ordovician Xiyangshan Formation; ∈ 1 h—lower Ordovician Hetang Formation; ηγ—monzonitic granite; ξγ—syenogranit; ①—Tongwu copper ore deposit in Guangde County; ②—Yangchong tungsten-molybdebnum ore deposit in Guangde County; ③—Bridgehead Xiqiling tungsten ore deposit in Ningguo City; ④—

 doi:10.20944/preprints202411.0865.v1

Dali Cu-Zn-Pb ore deposit in Ningguo City; ⑤—Shucun tungsten ore deposit in Ningguo City; ⑥—Lujiashan W-Be ore deposit in Ningguo City; ⑦—Wangcun Cu-Zn-Pb ore deposit in Ningguo City.

On the basis of carefully identifying various lithologic intrusions, fresh monzonitic granite (LC08-2, LC14, LC07, LC09) and granite (LC08-3, LC05, LC02-1) samples were collected from Liucun pluton. Representative samples monzonitic granite (LC08-2, LC14) and granite (LC08-3) were selected for mineralogical description (Figure 3).

Figure 3. Hand specimen photos and microscopic characteristics of Liucun pluton.Mineral abbreviations: Qtz-quartz; Kfs-K-feldspar; Pl-plagioclase; Bt-biotite.

LC14 (sampling coordinates 30°48′05″N, 119°21′51″E) is porphyritic biotite monzonitic granite with porphyritic structure, medium-grained to coarse-grained, massive structure. The main minerals are potassium feldspar 30～35%, plagioclase 20～25%, biotite 10～15%, quartz 20～25%. There is a small amount of accessory mineral zircon and magnetite. Quartz particles have biotite, weak strength alteration. Occasionally the phenomenon of mineral inclusion (feldspar inclusion of biotite), occasionally see zircon and other auxiliary minerals. Biotite, flaky, less, 0.5～1 mm. Quartz, round granular mesogranular structure. The quartz particle size can reach 0.5 ～2 mm, and the porphyry

 doi:10.20944/preprints202411.0865.v1

can reach 5mm. Potassium feldspar, plate columnar structure, semi-idiomorphic, particle size in 0.5 ～1.5mm, the largest up to 4mm. Plagioclase, polylamellar twin, long columnar porphyry columnar medium coarse-grained structure, more idiomorphic than potassium feldspar, particle size 0.5 ～ 2mm. Magnetite, steel gray, sparsely disseminated and stellate occurs in altered biotite. The crystal surface is uneven and has pits. The alteration is weak to moderate in intensity, mainly chlorite, sericite and weak clay alteration.

LC08-2 (sampling coordinates 30°44′29″N, 119°23′07″E), monzonitic granite, holocrystalline structure, coarse grained, massive structure, the main minerals are potassium feldspar 30～35%, plagioclase 25～30%, biotite 5～10%, quartz 20～25%. There is a small amount of accessory minerals and magnetite. Quartz grains have biotite, very little hornblende. The rocks are fresher. The mineral inclusion phenomenon was seen occasionally, and the minor minerals such as zircon, sphene were occasionally seen. Potassium feldspar, plate columnar structure, hemidiomorphic–idiomorphic, particle size of 0.5～2.5mm. Biotite, flaky, less, 1.5～2mm. Plagioclase, polylamellar twin-crystal, long columnar porphyry columnar medium coarse-grained structure, more idiomorphic than potassium feldspar, particle size 0.5～2.5mm. Quartz, round granular mesogranular structure. The quartz particle size can reach 0.5～4mm. Magnetite, steel gray, sparsely disseminated and stellate occurs in altered biotite. The crystal surface is uneven and has pits. Weak claying, and other alterations are weak.

LC08-3 (sampling coordinates 30°44′29″N, 119°23′07″E), weakly altered granite, holocrystalline structure, medium-coarse grained, massive structure, the main minerals are potassium feldspar 30～35%, plagioclase 20～25%, biotite 10～15%, quartz 15～20%. There is a small amount of accessory minerals and magnetite. Quartz particles have biotite, weak strength alteration. Mineral encrustment, zircon, sphene were occasionally seen. Potassium feldspar, plate columnar structure, hemidiomorphic, particle size of 0.5～3 mm. Plagioclase, long columnar porphyry columnar medium coarse-grained structure, more idiomorphic than potassium feldspar, particle size 2 ～ 3mm, individual 8mm. Biotite, flaky, less, 0.5～2 mm. Quartz, round granular mesogranular structure. The particle size of quartz can reach 1～2 mm. Magnetite, steel gray, sparsely disseminated and stellate occurs in altered biotite. The crystal surface is uneven and has pits. Medium intensity alteration, medium intensity chlorite, epidotite, weak sericite, and clay alteration.

3. Analytical Methods

3.1. Geochemical Analysis of Whole Rock

The analysis of major and trace elements of the whole rock was completed in Guangzhou Aosi Mineral Laboratory.

The major elements were analyzed by X-ray fluorescence spectrometry (XRF), and the analysis accuracy was better than 5%.

ICP-MS (Inductively coupled plasma mass spectrometry) was used to analyze trace and rare earth elements, and the analysis accuracy of most elements was better than 2%.

3.2. Sr-Nd Isotope Analysis of Whole Rock

The Sr-Nd isotope test was completed at the Laboratory of Solid Isotope Geochemistry, School of Earth and Space Sciences, University of Science and Technology of China. The instrument used was the Finnigan MAT262 multi-channel Mass Spectrometer (LA-MC-ICPMS). The isotopic ratios of Sr and Nd were determined using $^{87}Sr/^{88}Sr = 0.1194$ and $^{146}Nd/^{144}Nd = 0.7219$, respectively.

3.3. LA-ICP-MS Zircon U-Pb Dating

Zircon selection was completed in Langfang Dike Exploration Technology Service Co., LTD. Zircon target and cathode luminescence image photography are completed by Beijing Zirconia Linghang Technology Co., LTD.

 doi:10.20944/preprints202411.0865.v1

LA-ICP-MS Zircon U-Pb dating test was completed in Nanjing Jupu Detection Technology Co., LTD., using excimer laser ablation system Analyte Excite and quadrupole inductively coupled Plasma Mass Spectrometer (ICP-MS) model Agilent7700x.

3.4. Zircon Lu-Hf isotope

Zircon Lu-Hf isotope testing was performed at Nanjing Jupu Detection Technology Co., LTD., using the Nu Plasma II multi-receive plasma mass spectrometry and the Analyte Excite193nm AR-UV Laser Denudation system (LA-MC-ICP-MS).

4. Results

4.1. Results of Whole Rock Geochemical Analysis

4.1.1. Major Elements

The results of whole rock major and trace element analysis of Liucun pluton are shown in Table 1. The content of SiO_2 in monzonite granite ranges from 65.98% to 73.8%, with an average of 68.77%. The Al_2O_3 content was higher, ranging from 12.90% to 15.42%, with an average of 14.60%. The contents of K_2O and Na_2O were high, the average values were 4.56% and 3.35%, respectively. The total alkali content (Na_2O+K_2O) ranges from 7.66% to 8.07%. CaO content ranged from 1.23% to 2.76%, with an average of 2.12%. The contents of MgO ranged from 0.47% to 1.39%, with an average value of 1.06%. $Fe_2O_3^T$ content was low, ranging from 2.33% to 4.58%, with an average of 3.74%. The aluminum saturation index of Liucun monzonitic granite is high, with A/CNK ranging from 0.97 to 1.09 and A/NK ranging from 1.23 to 1.50. The content of SiO_2 in granite ranges from 64.79% to 76.67%, with an average of 71.38%. Al_2O_3 content was higher, ranging from 12.58% to 15.08%, with an average of 13.74%. The contents of K_2O and Na_2O were high, the average values were 4.71% and 3.39%, respectively. The total alkali content (Na_2O+K_2O) ranges from 7.64% to 8.47%. CaO content ranged from 0.61% to 3.03%, with an average of 1.67%. The MgO content ranged from 0.07% to 1.65%, with an average value of 1.06%. The content of $Fe_2O_3^T$ was low, ranging from 1.25% to 5.39%, with an average of 3.17%. The aluminum saturation index of Liucun granite is high, with A/CNK ranging from 0.95 to 1.04 and A/NK ranging from 1.13 to 1.47. The characteristics of major elements show that the Liucun pluton is all silica-rich, potassium-rich and peraluminous high potassium calc-alkaline rocks (Figure 4).

Table 1. Major (%) and trace element ($\times 10^{-6}$) concentrations of samples from the Liucun pluton.

Sample Number	LC07	LC08-2	LC09	LC14	LC02-1	LC05	LC08-3
Lithology		Monzonitic Granite				Granite	
SiO_2	66.76	73.8	65.98	68.55	72.67	76.67	64.79
TiO_2	0.57	0.25	0.65	0.52	0.31	0.06	0.73
Al_2O_3	15.31	12.9	15.42	14.75	13.56	12.58	15.08
$Fe_2O_3^T$	4.35	2.33	4.58	3.7	2.86	1.25	5.39
FeO	3.05	1.66	3.32	2.46	2.06	0.94	4.05
MnO	0.08	0.06	0.08	0.08	0.06	0.05	0.13
MgO	1.27	0.47	1.39	1.09	0.56	0.07	1.65
CaO	2.76	1.23	1.93	2.54	1.36	0.61	3.03
Na_2O	3.39	3.09	3.5	3.4	3.09	3.53	3.55
K_2O	4.27	4.98	4.45	4.55	5.09	4.94	4.09
P_2O_5	0.24	0.08	0.26	0.2	0.11	0.01	0.29
LOI	0.68	0.51	1.62	0.55	0.68	0.35	0.66
Total	102.73	101.36	103.18	102.39	102.41	101.06	103.44
Na_2O/K_2O	0.79	0.62	0.79	0.75	0.61	0.71	0.87
Na_2O+K_2O	7.66	8.07	7.95	7.95	8.18	8.47	7.64
A/CNK	1.00	1.01	1.09	0.97	1.04	1.02	0.95
A/NK	1.50	1.23	1.46	1.40	1.28	1.13	1.47
$Mg^{\#}$	0.31	0.24	0.32	0.32	0.23	0.08	0.31

 doi:10.20944/preprints202411.0865.v1

La	47.7	36.5	52.2	40.6	33.5	12.1	63.8
Ce	96.1	74.7	105	80.7	68.6	31.8	133.5
Pr	10.75	8.58	11.9	8.95	7.89	4.34	15.6
Nd	40.2	30.9	43.7	33.2	30.2	18.5	58.6
Sm	8.51	6.32	8.69	6.77	6.64	6.55	14
Eu	1.52	0.68	1.6	1.26	0.85	0.23	1.38
Gd	7.37	5.46	7.26	5.36	5.61	7.9	11.85
Tb	1.14	0.92	1.07	0.79	0.99	1.59	2.1
Dy	6.58	5.75	5.99	4.75	6.3	11.55	12.7
Ho	1.33	1.27	1.21	1	1.34	2.56	2.71
Er	3.85	4.03	3.53	2.75	3.93	8.33	7.93
Tm	0.54	0.64	0.51	0.42	0.65	1.39	1.23
Yb	3.79	4.54	3.47	2.84	4.66	10.15	8.4
Lu	0.59	0.74	0.55	0.47	0.71	1.53	1.27
Sc	8.3	3.8	8.6	6.3	5.3	3.1	11.8
V	58	20	57	48	27	3	74
Cr	30	20	20	30	20	20	30
Co	7.3	2.6	7	5.4	3.4	0.5	8.9
Ni	7.2	2.7	7.1	4.9	3.2	0.9	8.5
Ga	19.4	15.1	17.8	16.8	17	16.65	21.1
Rb	157.5	237	145.5	157	201	319	202
Sr	308	107.5	303	292	160	24.9	267
Y	36.9	35.4	29.2	25.7	36.9	58.4	74.6
Zr	267	145	303	230	211	89	363
Nb	18.4	18.3	20	16.5	15.9	26.1	34.8
Ba	841	333	1025	835	554	32.9	757
Hf	6.9	4.6	7.8	6	5.8	4.3	9.4
Ta	1.3	2.1	1.1	1.3	1.5	3.8	2.4
Pb	19	25.3	18.6	19.1	25.4	39.2	19
Th	12.15	19.4	13.75	13.85	12.1	21.8	14.65
U	2.9	7.1	2.9	3.2	4.6	12.3	3
∑REE	229.97	181.03	246.68	189.86	171.87	118.52	335.07
∑LREE	204.78	157.68	223.09	171.48	147.68	73.52	286.88
∑HREE	25.19	23.35	23.59	18.38	24.19	45.00	48.19
LREE/HREE	8.13	6.75	9.46	9.33	6.11	1.63	5.95
(La/Yb）N	9.03	5.77	10.79	10.25	5.16	0.86	5.45
δEu	0.59	0.35	0.62	0.64	0.43	0.10	0.33
δCe	1.04	1.03	1.03	1.04	1.03	1.08	1.04

Notes: A/NK =Al_2O_3/(Na_2O+K_2O) (mol); A/CNK = Al_2O_3/(CaO+Na_2O+K_2O) (mol); $Mg^{\#}$=MgO/(MgO+FeO+Fe_2O_3) (mol).

 doi:10.20944/preprints202411.0865.v1

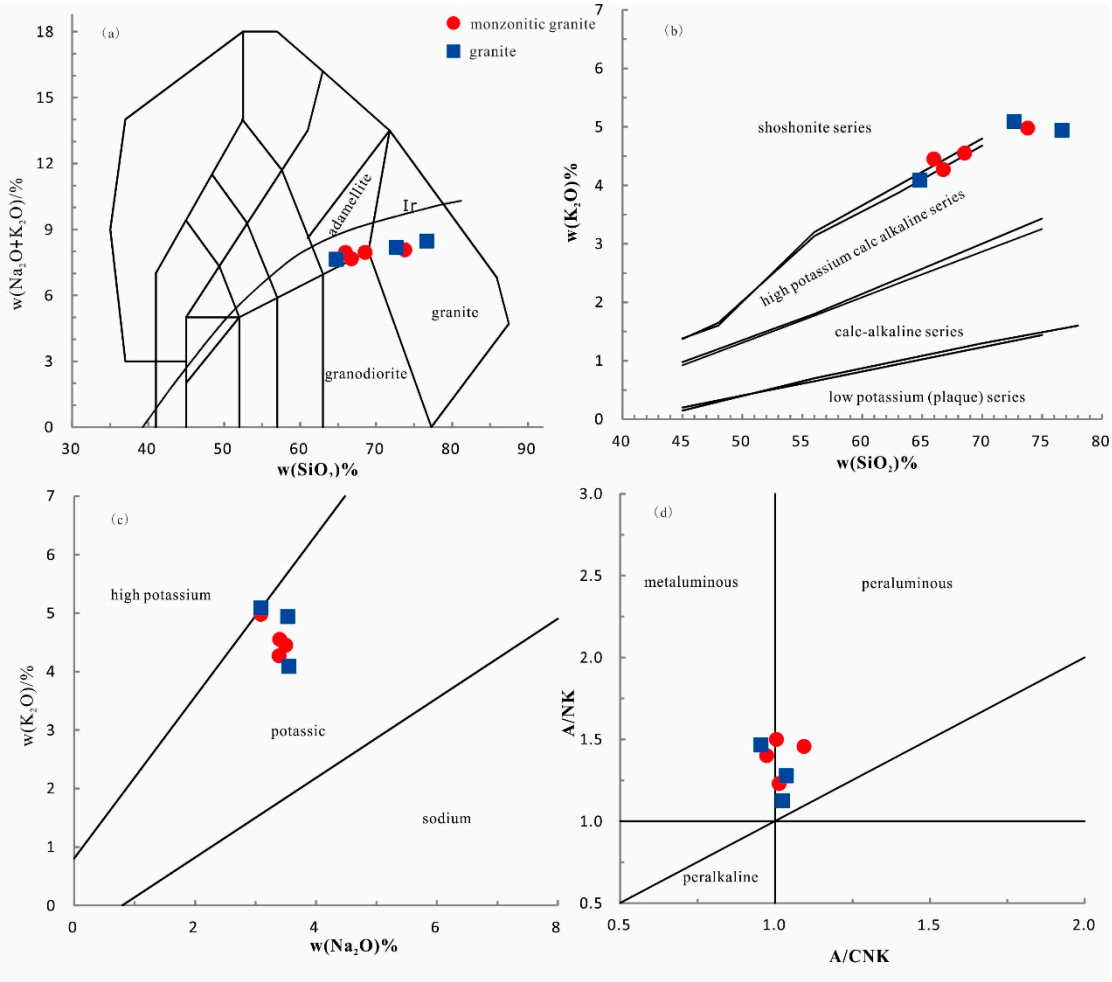

Figure 4. The whole rock discriminative diagrams of samples from the Liucun pluton.

According to the Haker diagram (Figure 5), SiO_2 of monzonite and granite has a good correlation with the remaining oxides, and the content of SiO_2 is negatively correlated with the content of TiO_2, Fe_2O_3, MgO, CaO, P_2O_5 and MnO, and positively correlated with the content of K_2O.

 doi:10.20944/preprints202411.0865.v1

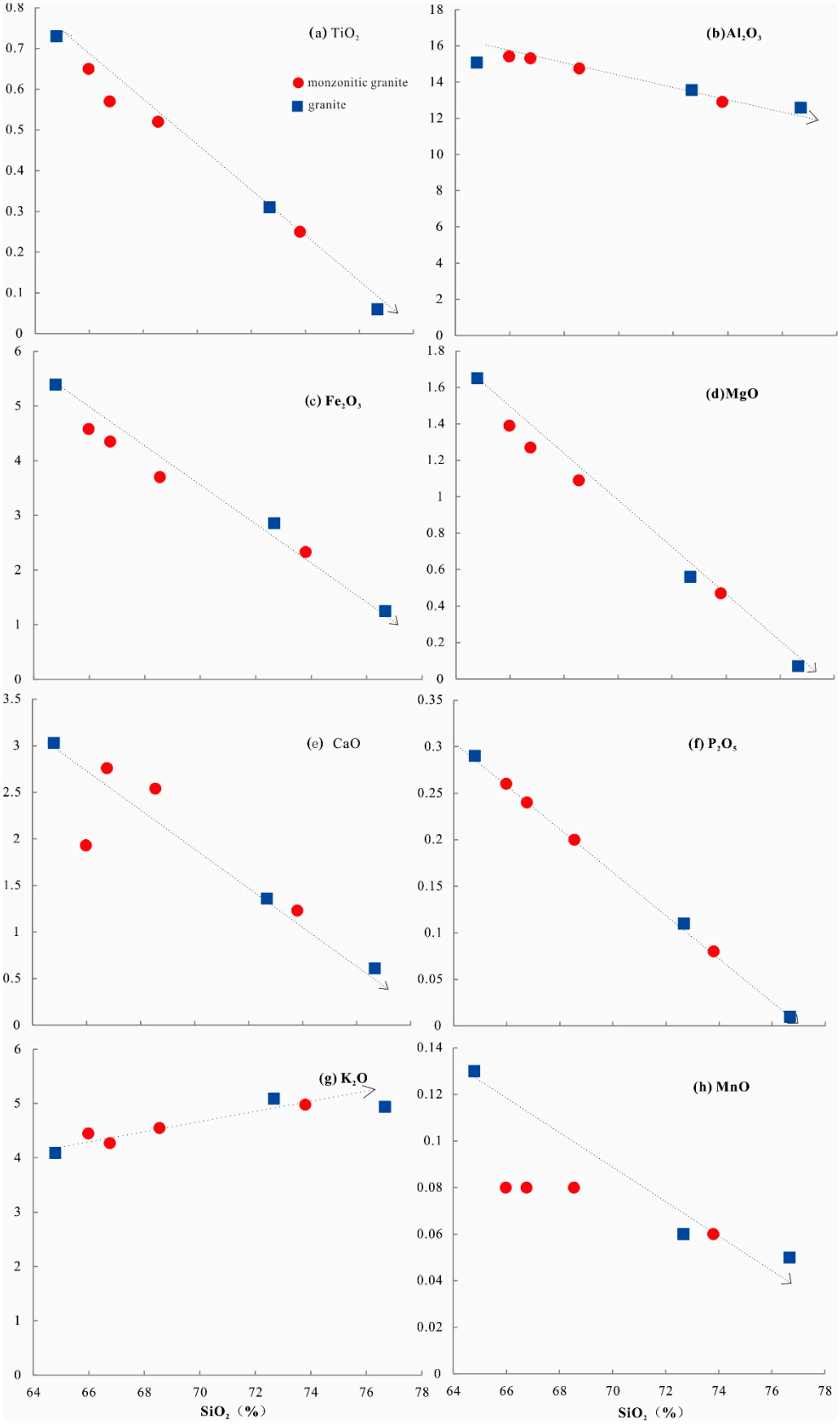

Figure 5. Diagrams of SiO_2 vs. major elements of monzonitic granite and granite from Liucun pluton.

 doi:10.20944/preprints202411.0865.v1

4.1.2. Rare Earth and Trace Elements

∑REE of monzogranite ranges from 181.03×10⁻⁶ to 246.68×10⁻⁶, LREE/HREE ratio from 6.75 to 9.46, $(La/Yb)_N$ ratio from 5.77 to 10.79, δEu from 0.35 to 0.64. ∑REE of granite is 118.52×10⁻⁶～335.07×10⁻⁶, LREE/HREE ratio is 1.63～6.11, $(La/Yb)_N$ ratio is 0.86～5.45, δEu is 0.10～0.43. The chondrite-normalized patterns show that the magmatic rocks of Liucun complex pluton all have right-leaning characteristics of light rare earth element enrichment and heavy rare earth element deficit, and the degree of differentiation of light and heavy rare earth element is similar, with obvious negative Eu anomaly. Monzonitic granite has stronger right-leaning characteristics than granite. The contents of Cr and Ni in samples are low, ranging from 20×10⁻⁶ to 30×10⁻⁶ and 0.9×10⁻⁶ to 8.5×10⁻⁶, respectively, which are much lower than the original mantle magmatic values (Cr > 1000×10⁻⁶, Ni > 400×10⁻⁶, after the paper [26]). It suggests that the magma has undergone a high degree of evolution or the source region is not dominated by the mantle.

The primitive mantle-normalized spider diagrams show that the trace elements curves of monzonitic granite and granite in Liucun complex pluton are similar, showing the enrichment of large ion lithophilic elements (LILE) such as Rb and Ba, and the depletion of high field strength elements (HFSE) such as Nb, Ta and Ce (Figure 6).

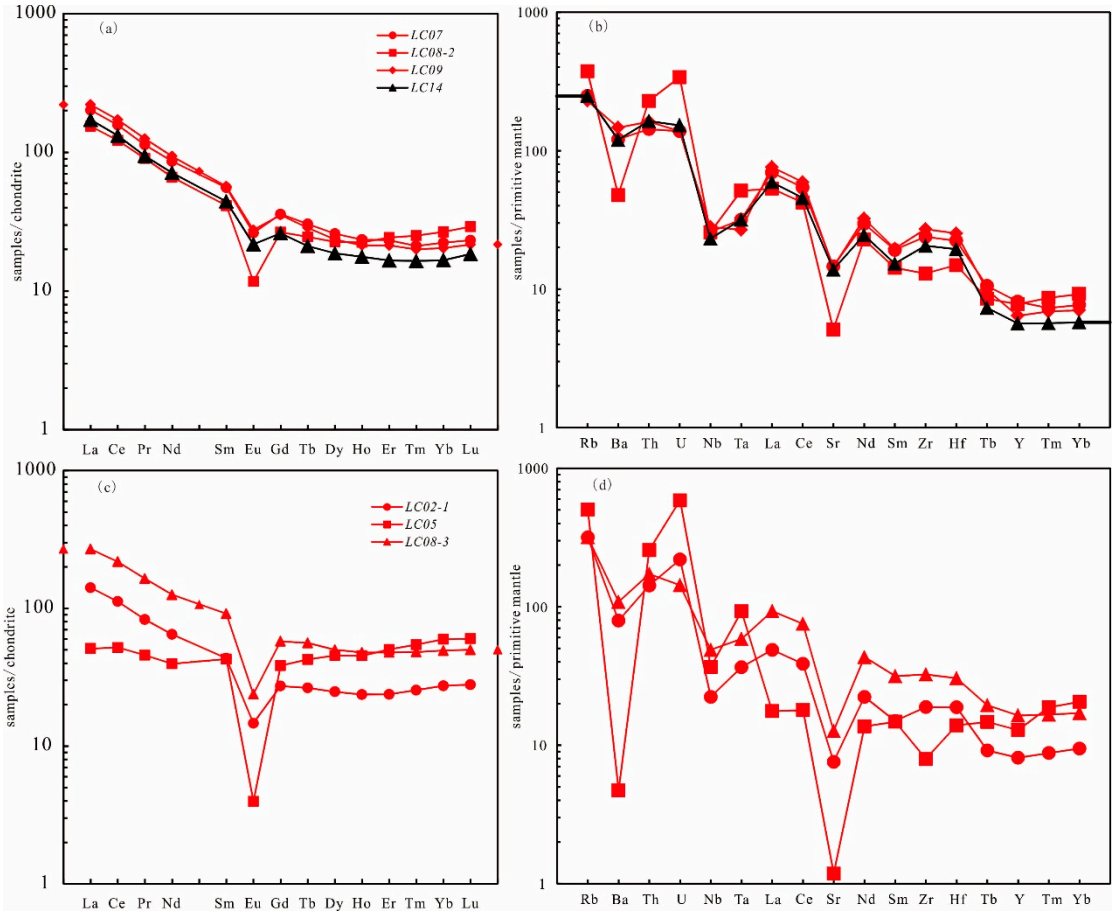

Figure 6. REE chondrite-normalized patterns(a,c) and primitive mantle-normalized spider diagrams(b,d)of the granodiorite and pegmatite from Liucun pluton(normalization values after the paper [27]).

In recent years, scholars have paid attention to the general enrichment of rare earth elements in granite weathering crust in southern Anhui province, which has become a deposit in some areas [28]. The concentration of rare earth elements in weathering crust of Liucun pluton is also very high, and the enrichment of rare earth elements deserves further research.

 doi:10.20944/preprints202411.0865.v1

4.2. Whole Rock Sr-Nd Isotope

Sr-Nd isotope analysis of monzonitic granite (LC08-2), porphyritic biotite monzonitic granite (LC14) and granite (LC08-3) in Liucun pluton was conducted, and the experimental results are listed in Table 2.

The results show that the Sr-Nd isotopic characteristics of the three samples from Liucun pluton are similar, which shows the characteristics of homologous magma. The $^{87}Sr/^{86}Sr$ values of monzonite are 0.711987～0.720512, the $^{87}Sr/^{86}Sr$ values of granites are 0.713192, and the ε_{Nd} (t) values of monzonite (-4.7～ -2.42) are slightly lower than those of granites (-1.74). The $^{143}Nd/^{144}Nd$ values of the two are very similar, ranging from 0.512335 to 0.512503, and the initial $^{87}Sr/^{86}Sr$ (I_{Sr}) is in the same range, ranging from 0.70904 to 0.70934. The depleted mantle model ages (T_{DM2}) are 1122～1306Ma (monzonitic granite) and 1069Ma (granite), respectively.

4.3. LA-ICP-MS U-Pb Isotope Age of Zircon

Zircon LA-ICP-MS U-Pb dating results of monzonitic granite and granites in the Liucun complex pluton are shown in Table 3. The zircon grains have good idiomorphic crystal and clear oscillating zone, which are magmatic zircons. The measured age values represent the formation age of the rock.

The $^{206}Pb/^{238}U$ ages of 20 zircons (17 effective sites) from the monzonite granite (LC08-2) range from 121.4 to 142.4Ma, with a weighted average age of 130.50±0.55Ma (MSWD=1.18) (Figure 7). The $^{206}Pb/^{238}U$ ages of 20 zircons (17 effective sites) from porphyritic biotica monzonite granite (LC14) range from 126.8 to 147.7Ma, with a weighted mean age of 128.95±0.46Ma (MSWD=1.12) (Figure 7). The $^{206}Pb/^{238}U$ ages of 20 zircons (12 effective measurement sites) from the granite (LC08-3) range from 126.7 to 161.8Ma, with a weighted average age of 133.85±0.45Ma (MSWD=5.4) (Figure 7).

Table 2. Sr-Nd isotopic compostions of the monzonitic granite and granite from Liucun pluton.

Sample number	lithology	t (Ma)	Rb	Sr	$^{87}Rb/^{86}Sr$	$^{87}Sr/^{86}Sr$	2σ	Sm	Nd	$^{147}Sm/^{144}Nd$	$^{143}Nd/^{144}Nd$	2σ	I_{Nd} (t)	I_{Sr} (t)	ε_{Nd} (t)	T_{DM2} (Ma)
			(×10⁻⁶)					(×10⁻⁶)								
LC08-2	monzonitic granite	130.5	237	114	6.022	0.720512	0.000010	6.32	30.9	0.1236	0.512452	0.000011	0.512346	0.70934	-2.42	1122
LC14	biotite monzogranite	128.95	157	300	1.515	0.711987	0.000015	6.77	33.2	0.1233	0.512335	0.000010	0.512231	0.70921	-4.7	1306
LC08-3	granite	133.5	202	267	2.190	0.713192	0.000012	14.00	58.6	0.1444	0.512503	0.000007	0.512377	0.70904	-1.74	1069

Note: Constants used in the calculations are: λ_{Sm} = 6.54 × 10-12; λ_{Rb} = 1.42 × $^{10-12}$. deficit mantle (DM): $^{147}Sm/^{144}Nd$ = 0.2136, $^{143}Nd/^{144}Nd$ = 0.513151. deficit mantle model age (T_{DM2}) was calculated using the model of the paper [29].

 doi:10.20944/preprints202411.0865.v1

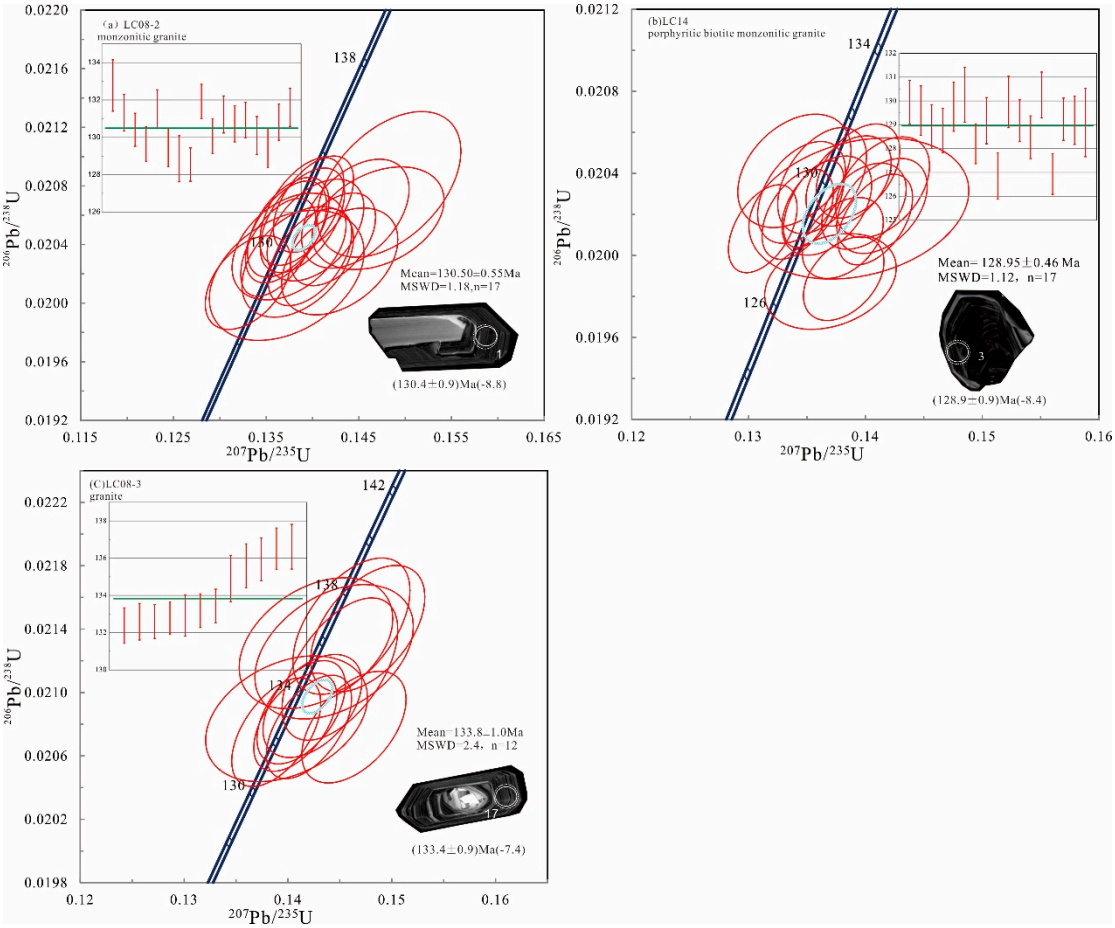

Figure 7. U-Pb concordant plots of zircon and cathodoluminescence images showing characteristics of representative zircons from the Liucun pluton (The number in the zircon cathode luminescence image represents the point number, the solid coil is the U-Pb age measuring point, and the dashed coil is the Hf isotope analysis point).

3.4. Lu-Hf Isotope Characteristics of Zircon

The results of zircon Lu-Hf isotope testing of monzonitic granite and granite samples from Liucun complex pluton are shown in Table 4. The $^{176}Lu/^{177}Hf$ ratio of the zircons measured in this study is less than 0.002 except for a few points which slightly exceed 0.002, indicating low radiogenic Hf accumulation after zircon formation [30]. The $^{176}Lu/^{177}Hf$ and $^{176}Hf/^{177}Hf$ values of the 17 zircons from the monzonite granite (LC08-2) range from 0.001168 to 0.002417 and from 0.282430 to 0.282499, respectively. ε_{Hf} (t) value is between -9.3 and -6.9; The T_{DM2} model age ranges from 1618 to 1771Ma. The $^{176}Lu/^{177}Hf$ and $^{176}Hf/^{177}Hf$ values of 15 zircons from porphyritic biotite monzonite (LC14) are between 0.000852 and 0.002410 and 0.282429 and 0.282467, respectively. ε_{Hf} (t) value is between -9.4 and -8.0; The T_{DM2} model age ranges from 1687 to 1774Ma. The $^{176}Lu/^{177}Hf$ and $^{176}Hf/^{177}Hf$ values of the 16 zircons from the granite (LC08-3) range from 0.001034 to 0.002167 and from 0.282385 to 0.282484, respectively. ε_{Hf} (t) value is between -10.9 and -7.4; The T_{DM2} model age ranges from 1651 to 1840Ma.

 doi:10.20944/preprints202411.0865.v1

Table 3. U-Pb dating results of zircon from the Liucun pluton.

Test point	Content (μg/g)		Th/U	Isotope Ratio						Age (Ma)			
	Th	U		$^{207}Pb/^{206}Pb$	1σ	$^{207}Pb/^{235}U$	1σ	$^{206}Pb/^{238}U$	1σ	$^{207}Pb/^{235}U$	1σ	$^{206}Pb/^{238}U$	1σ
Monzonitic Granite (LC08-2)													
LC08-2-01	310.26	880.68	0.35	0.050363	0.000675	0.142208	0.002024	0.020436	0.000139	135.0	1.8	130.4	0.9
LC08-2-02	127.72	286.21	0.45	0.052146	0.001227	0.148254	0.003412	0.020811	0.000219	140.4	3.0	132.8	1.4
LC08-2-03	265.91	1151.47	0.23	0.049838	0.000673	0.139726	0.001983	0.020314	0.000146	132.8	1.8	129.6	0.9
LC08-2-04	411.17	714.02	0.58	0.050719	0.000819	0.144621	0.002552	0.020611	0.000163	137.2	2.3	131.5	1.0
LC08-2-05	98.66	539.91	0.18	0.051165	0.000940	0.142935	0.002762	0.020285	0.000160	135.7	2.5	129.5	1.0
LC08-2-07	86.27	228.30	0.38	0.049576	0.001360	0.137211	0.003673	0.020190	0.000195	130.6	3.3	128.9	1.2
LC08-2-08	216.33	1077.78	0.20	0.047882	0.000732	0.133046	0.002033	0.020140	0.000140	126.8	1.8	128.5	0.9
LC08-2-09	123.29	466.18	0.26	0.051557	0.001036	0.147076	0.003130	0.020580	0.000154	139.3	2.8	131.3	1.0
LC08-2-10	252.85	1208.57	0.21	0.049078	0.000638	0.140101	0.001904	0.020675	0.000145	133.1	1.7	131.9	0.9
LC08-2-11	304.63	1576.02	0.19	0.048461	0.000591	0.136312	0.001787	0.020381	0.000147	129.8	1.6	130.1	0.9
LC08-2-12	319.17	1239.07	0.26	0.048918	0.000650	0.138907	0.002003	0.020565	0.000157	132.1	1.8	131.2	1.0
LC08-2-13	254.06	1262.64	0.20	0.048533	0.000642	0.137148	0.001925	0.020486	0.000153	130.5	1.7	130.7	1.0
LC08-2-14	324.77	1116.43	0.29	0.048508	0.000643	0.137377	0.001936	0.020518	0.000150	130.7	1.7	130.9	0.9
LC08-2-15	119.08	830.69	0.14	0.048903	0.000885	0.137470	0.002706	0.020387	0.000160	130.8	2.4	130.1	1.0
LC08-2-16	98.00	500.82	0.20	0.049725	0.000951	0.138404	0.002648	0.020281	0.000166	131.6	2.4	129.4	1.1
LC08-2-18	151.61	672.57	0.23	0.049484	0.000748	0.140317	0.002297	0.020499	0.000153	133.3	2.0	130.8	1.0
LC08-2-19	326.97	1282.61	0.25	0.048769	0.000631	0.138848	0.001992	0.020626	0.000162	132.0	1.8	131.6	1.0
porphyritic biotite monzonitic granite (LC14)													
LC14-01	390.27	816.24	0.48	0.049287	0.000827	0.138566	0.002407	0.020363	0.000145	131.8	2.1	129.9	0.9
LC14-02	180.08	520.04	0.35	0.048164	0.000873	0.134536	0.002478	0.020307	0.000164	128.2	2.2	129.6	1.0
LC14-03	254.79	838.54	0.30	0.048314	0.000716	0.134207	0.002016	0.020200	0.000145	127.9	1.8	128.9	0.9
LC14-04	310.52	997.11	0.31	0.050644	0.000729	0.140847	0.002110	0.020175	0.000146	133.8	1.9	128.8	0.9
LC14-05	264.33	651.02	0.41	0.050359	0.000873	0.141477	0.002651	0.020332	0.000162	134.4	2.4	129.8	1.0
LC14-06	107.41	351.89	0.31	0.047631	0.001104	0.133922	0.003197	0.020412	0.000182	127.6	2.9	130.3	1.2
LC14-08	842.67	741.75	1.14	0.049784	0.000816	0.138074	0.002288	0.020085	0.000130	131.3	2.0	128.2	0.8
LC14-09	279.40	558.43	0.50	0.050595	0.000863	0.141421	0.002559	0.020241	0.000153	134.3	2.3	129.2	1.0
LC14-10	288.41	291.20	0.99	0.050337	0.001418	0.137015	0.003717	0.019872	0.000154	130.4	3.3	126.8	1.0
LC14-12	213.19	583.51	0.37	0.048467	0.000850	0.136299	0.002509	0.020365	0.000170	129.7	2.2	130.0	1.1
LC14-14	220.21	542.73	0.41	0.050189	0.000880	0.139886	0.002385	0.020240	0.000138	132.9	2.1	129.2	0.9
LC14-15	379.17	825.54	0.46	0.047007	0.000622	0.131217	0.001938	0.020130	0.000141	125.2	1.7	128.5	0.9
LC14-16	254.24	617.85	0.41	0.049446	0.000818	0.139367	0.002364	0.020411	0.000151	132.5	2.1	130.3	1.0
LC14-17	355.91	636.50	0.56	0.050432	0.000836	0.138147	0.002275	0.019886	0.000135	131.4	2.0	126.9	0.9
LC14-18	160.97	1001.76	0.16	0.048598	0.000631	0.135582	0.001706	0.020250	0.000140	129.1	1.5	129.2	0.9
LC14-19	172.69	524.79	0.33	0.049145	0.000891	0.136698	0.002536	0.020242	0.000159	130.1	2.3	129.2	1.0
LC14-20	37.66	81.67	0.46	0.051449	0.002376	0.139445	0.006213	0.020228	0.000227	132.5	5.5	129.1	1.4
granite (LC08-3)													
LC08-3-01	386.53	1309.97	0.30	0.049566	0.000611	0.142028	0.001805	0.020782	0.000144	134.8	1.6	132.6	0.9
LC08-3-02	341.87	862.40	0.40	0.049623	0.000729	0.145009	0.002452	0.021147	0.000198	137.5	2.2	134.9	1.2
LC08-3-03	140.91	839.95	0.17	0.051072	0.000766	0.146360	0.002207	0.020781	0.000155	138.7	2.0	132.6	1.0
LC08-3-04	114.04	282.40	0.40	0.048622	0.001074	0.142701	0.003254	0.021311	0.000182	135.4	2.9	135.9	1.1
LC08-3-09	210.01	628.17	0.33	0.049348	0.000742	0.146119	0.002480	0.021418	0.000189	138.5	2.2	136.6	1.2
LC08-3-12	133.51	241.64	0.55	0.048753	0.001168	0.139869	0.003430	0.020834	0.000175	132.9	3.1	132.9	1.1
LC08-3-14	204.56	721.18	0.28	0.049995	0.000786	0.147684	0.002420	0.021402	0.000175	139.9	2.1	136.5	1.1
LC08-3-15	110.58	284.74	0.39	0.049597	0.001151	0.144450	0.003356	0.021257	0.000186	137.0	3.0	135.6	1.2
LC08-3-16	181.80	962.05	0.19	0.049042	0.000613	0.140709	0.001758	0.020812	0.000136	133.7	1.6	132.8	0.9
LC08-3-17	266.94	920.53	0.29	0.049328	0.000701	0.142354	0.002092	0.020914	0.000143	135.1	1.9	133.4	0.9
LC08-3-18	272.80	1063.26	0.26	0.048549	0.000644	0.138877	0.001886	0.020748	0.000151	132.0	1.7	132.4	1.0
LC08-3-19	461.70	1181.58	0.39	0.049123	0.000641	0.141275	0.001872	0.020875	0.000143	134.2	1.7	133.2	0.9

Table 4. Lu-Hf isotopic compositions of zircon from the Liucun pluton.

Test Point	$^{176}Yb/^{177}Hf$	$^{176}Lu/^{177}Hf$	2σ	$^{176}Hf/^{177}Hf$	2σ	Age (Ma)	$\varepsilon_{Hf}(t)$	T_{DM1}	T_{DM2}	$f_{Lu/Hf}$
LC08-2				monzonitic granite						
LC08-2-1	0.034666	0.001297	0.000004	0.282445	0.000008	130.4	-8.81	1150	1747	-0.96
LC08-2-2	0.042051	0.001507	0.000012	0.282454	0.000009	132.8	-8.44	1143	1726	-0.95
LC08-2-3	0.032602	0.001284	0.000011	0.282460	0.000011	129.6	-8.3	1128	1713	-0.96
LC08-2-4	0.066740	0.002417	0.000016	0.282455	0.000008	131.5	-8.54	1170	1728	-0.93
LC08-2-5	0.028864	0.001168	0.000006	0.282472	0.000008	129.5	-7.84	1107	1685	-0.96
LC08-2-7	0.054482	0.002058	0.000023	0.282477	0.000010	128.9	-7.78	1127	1679	-0.94
LC08-2-8	0.038874	0.001476	0.000003	0.282455	0.000007	128.5	-8.5	1141	1726	-0.96
LC08-2-9	0.028752	0.001086	0.000005	0.282438	0.000008	131.3	-9.04	1153	1761	-0.97
LC08-2-10	0.044404	0.001668	0.000010	0.282446	0.000007	131.9	-8.78	1159	1744	-0.95
LC08-2-11	0.033442	0.001169	0.000004	0.282499	0.000008	130.1	-6.91	1070	1626	-0.96
LC08-2-12	0.061627	0.002264	0.000011	0.282450	0.000008	131.2	-8.72	1173	1740	-0.93
LC08-2-13	0.042694	0.001616	0.000013	0.282482	0.000011	130.7	-7.53	1107	1665	-0.95
LC08-2-14	0.051891	0.001905	0.000024	0.282464	0.000008	130.9	-8.2	1142	1708	-0.94
LC08-2-15	0.034133	0.001362	0.000023	0.282466	0.000007	130.1	-8.11	1123	1702	-0.96
LC08-2-16	0.041585	0.001635	0.000005	0.282458	0.000007	129.4	-8.41	1141	1719	-0.95
LC08-2-18	0.032475	0.001197	0.000007	0.282430	0.000008	130.8	-9.33	1168	1780	-0.96

 doi:10.20944/preprints202411.0865.v1

LC08-2-19	0.037640	0.001441	0.000001	0.282454	0.000009	131.6	-8.47	1141	1726	-0.96
LC14	porphyritic biotite monzonitic granite									
LC14-2	0.029774	0.001261	0.000019	0.282429	0.000011	129.6	-9.43	1172	1784	-0.96
LC14-3	0.034529	0.001316	0.000014	0.282458	0.000009	128.9	-8.42	1133	1720	-0.96
LC14-4	0.027043	0.001151	0.000005	0.282456	0.000008	128.8	-8.46	1130	1723	-0.97
LC14-5	0.032517	0.001319	0.000013	0.282443	0.000012	129.8	-8.9	1153	1751	-0.96
LC14-6	0.020863	0.000881	0.000008	0.282467	0.000009	130.3	-8	1106	1695	-0.97
LC14-8	0.063363	0.002410	0.000039	0.282435	0.000009	128.2	-9.28	1199	1775	-0.93
LC14-9	0.032816	0.001255	0.000013	0.282452	0.000008	129.2	-8.59	1139	1732	-0.96
LC14-10	0.065406	0.002145	0.000024	0.282440	0.000011	126.8	-9.14	1184	1765	-0.94
LC14-12	0.025735	0.001029	0.000004	0.282453	0.000008	130.0	-8.5	1130	1727	-0.97
LC14-14	0.030085	0.001126	0.000002	0.282450	0.000008	129.2	-8.63	1137	1735	-0.97
LC14-15	0.054421	0.002017	0.000024	0.282458	0.000008	128.5	-8.43	1153	1721	-0.94
LC14-16	0.030100	0.001146	0.000006	0.282434	0.000009	130.3	-9.2	1160	1770	-0.97
LC14-17	0.033861	0.001266	0.000004	0.282437	0.000008	126.9	-9.17	1159	1765	-0.96
LC14-18	0.037303	0.001363	0.000024	0.282439	0.000006	129.2	-9.05	1160	1761	-0.96
LC14-19	0.021867	0.000871	0.000005	0.282456	0.000009	129.2	-8.41	1122	1721	-0.97
LC14-20	0.022815	0.000852	0.000008	0.282462	0.000008	129.1	-8.2	1112	1706	-0.97
LC08-3	granite									
LC08-3-1	0.048070	0.001768	0.000012	0.282449	0.000011	132.6	-8.66	1158	1738	-0.95
LC08-3-2	0.056244	0.002167	0.000014	0.282471	0.000008	134.9	-7.9	1140	1691	-0.93
LC08-3-3	0.032200	0.001130	0.000005	0.282447	0.000009	132.6	-8.69	1142	1740	-0.97
LC08-3-4	0.040687	0.001444	0.000006	0.282467	0.000009	135.9	-7.95	1123	1695	-0.96
LC08-3-5	0.044623	0.001654	0.000011	0.282435	0.000009	139.5	-9	1175	1766	-0.95
LC08-3-7	0.058329	0.001968	0.000024	0.282427	0.000007	146.6	-9.16	1196	1780	-0.94
LC08-3-9	0.045140	0.001562	0.000006	0.282440	0.000010	136.6	-8.89	1165	1756	-0.95
LC08-3-11	0.031283	0.001173	0.000007	0.282448	0.000009	138.2	-8.53	1141	1734	-0.96
LC08-3-12	0.039362	0.001497	0.000004	0.282449	0.000009	132.9	-8.65	1151	1738	-0.95
LC08-3-13	0.027196	0.001034	0.000005	0.282465	0.000010	127.1	-8.14	1114	1703	-0.97
LC08-3-14	0.048543	0.001794	0.000026	0.282474	0.000009	136.5	-7.72	1124	1681	-0.95
LC08-3-15	0.029626	0.001201	0.000009	0.282482	0.000007	135.6	-7.39	1095	1661	-0.96
LC08-3-16	0.043622	0.001730	0.000009	0.282482	0.000012	132.8	-7.48	1110	1664	-0.95
LC08-3-17	0.041481	0.001674	0.000007	0.282484	0.000008	133.4	-7.4	1105	1658	-0.95
LC08-3-18	0.031496	0.001274	0.000006	0.282385	0.000010	132.4	-10.93	1234	1880	-0.96
LC08-3-19	0.054329	0.002152	0.000023	0.282462	0.000009	133.2	-8.25	1152	1711	-0.94

5. Discussion

5.1. Diagenetic Age of Liucun Pluton and Mesozoic Magmatic Rock Age Framework in Southern Anhui Province

The LA-ICP-MS U-Pb weighted mean ages of zircons from monzonitic granite and porphyritic biotite monzonitic granite in Liucun pluton are 130.50±0.55Ma and 128.95±0.46Ma, respectively. The age data of all measuring points are concentrated in the small variation range of 5Ma, indicating that these zircons are the products of the same magmatic event. The weighted mean age indicates the emplacement time of the monzonite granite. This age is consistent with the previous obtained formation ages of monzonitic granite in the Liucun pluton of 129.0±1.0Ma, 129.7±2.1Ma [31], 132.84±0.57Ma [15] and 124.4±1.0Ma [16].

The LA-ICP-MS U-Pb weighted mean age of the granite zircon is 133.8±1.0Ma, which is larger than that of the monzonitic granite.

The Xianxia, Yaocun and Miaxi plutons surrounding the Liucun pluton have been tested for isotopic age in the past. Among them, the Xianxia complex pluton monzonitic granite (143.0±3.5Ma), granodiorite (140.0±2.0Ma) and potassium feldspar granite (138.6±3.5Ma) [32]. Yaocun pluton granite (127.6±1.4Ma, 127.9±1.4Ma) [28,33], Miaoxi pluton monzonitic granite (128.2±1.5Ma), syenite granite (124.9±1.5Ma) [34]. The age of Liucun pluton is consistent with that of Miaoxi pluton and Yaocun pluton, and younger than that of Xianxia pluton.

The large-scale magmatism in the magmatic belt of southern Anhui mainly occurred in the late Yanshanian period, often in the form of large batholith and complex pluton. According to the rock type, distribution, isotopic geological age and metallogenic characteristics of magmatic rocks, the Yanshanian magmatism can be divided into two stages: early and late. In the early stage (152～135Ma), the lithology is granodiorite (porphyry), monzonitic granite, granite (porphyry) rock, granitic rock lithology is mostly granodiorite, the rocks are neutral. There are two types of emplacement pluton. One is shallow emplacement plutons, mostly produced by small rock strains,

 doi:10.20944/preprints202411.0865.v1

which is related to tungsten and molybdenum polymetallic mineralization. The lithology includes granodiorite porphyry and granite (porphyry) rock, such as Dongyuan, Xiaoyao, Kaobeijian and Lidongkeng pluton. The other is the deep emplacement plutons, which are mainly composed of large batholith and complex intrusions. The lithology is mainly granodiorite, such as Qingyang, Chengan, Langqiao, Jingde and Taiping pluton. In the late stage (135～122Ma), it is mainly complex intrusive pluton, mostly monzonitic granite, syenite granite, granite porphyry, etc., most of which have A-type granite characteristics, such as Jiuhuashan, Huangshan, Fuling, Liucun pluton, etc [2,31,35,36]. This is basically consistent with the statement of the paper [37], who analyzed the Yanshanian granite data in southern Anhui and neighboring areas and concluded that the early (150～132Ma) and late (132～120Ma) stages were divided by 132Ma as the boundary.

Through the induction and analysis of the diagenetic data of two periods of magmatic activity in the late Mesozoic period in southern Anhui, it can be found that the lithology of early granitic rocks (152～135Ma) is mostly granodiorite. Late (135～122Ma) lithology is dominated by granite and syenite-granite (Figure 8). The early granodiorite is often closely related to mineralization, and many large and medium-sized W, Mo, Cu and Au deposits have been found. The deposits associated with late granites are rare. More than 70 deposits discovered in Jiangnan Orogenic belt (Anhui section) are related to Yanshanian magmatism, and the main mineral species are W, Mo, Pb-Zn, Cu and Au. In addition, a large number of extrusive rocks such as rhyolite developed in the Mesozoic in southern Anhui.

The Liucun pluton is the product of late magmatic activity in Jiangnan uplift belt, and the emplacement time of granite is slightly earlier than that of monzonitic granite.

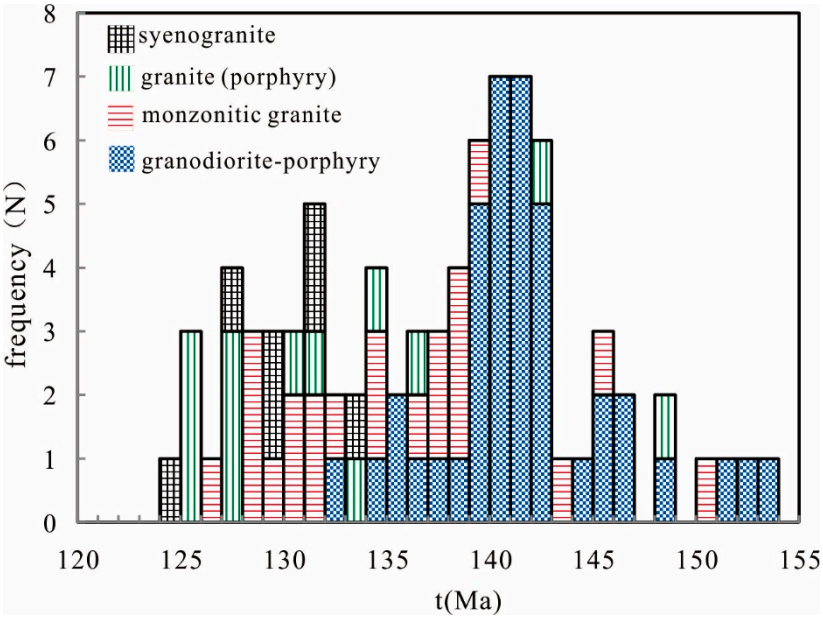

Figure 8. Age histogram of Mesozoic intrusive rocks in southern Anhui. Data from the papers [8,11,25,28,31–36,38–46], and my unpublished data.

5.2. Geochemical Properties and Petrogenesis

According to different source rock properties, granites are generally classified into type I, type S and type M [47,48], and A-type granites were first proposed by the paper [49] to define a class of Alkaline, Anhydrous, and non-orogenic granites, which have special geochemical characteristics. The Liucun pluton in southern Anhui province has high content of Na_2O+K_2O, high content of high field strength elements and rare earth elements, strong loss of Sr and Eu, and enrichment of Yb. These geochemical characteristics are similar to typical A-type granites [47–50]. In the Na_2O-K_2O diagram, all the sample points fall in the A-type granite region (Figure 9a), but in the ZR-10000Ga/Al diagram, there are 3 points in the A-type granite region, there are 3 points near the dividing line between A-type granite and I-type granite (Figure 9b), which may have advanced magmatic evolution, and the

 doi:10.20944/preprints202411.0865.v1

reason maybe is the increase in the degree of material assimilation and mixing in the upper crust is related to the decrease in the abundance of high field strength elements [39]. In addition, the rare earth element fractionation model table of Liucun pluton also shows a strong negative Eu anomaly characteristic of A-type granite. Therefore, the Liucun pluton has typical A-type granite characteristics, and comprehensive analysis shows that it belongs to A-type granite.

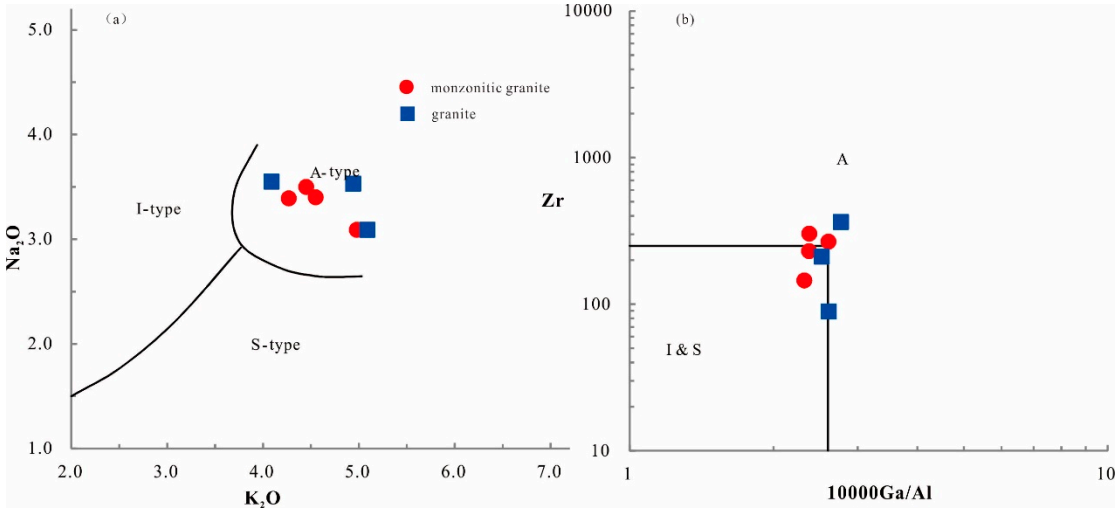

Figure 9. Na_2O-K_2O discriminant map (a,after the paper [51]) and Zr- (10000Ga/Al) discriminant map (b, after the paper [47]) of Liucun pluton.

Previous studies on the genesis of early Mesozoic (152～135Ma) granitic rocks (mainly granodiorite, rock type I/S type) in the eastern section of Jiangnan Orogenic belt are consistent, and basically agree that the magma source area is not only dominated by shell source, but also ancient crustal material plays an important role [5,38,39]. However, the genesis of late (135～122Ma) granitic pluton(mainly granite and syenite-granite, rock type A) still has a dispute between mantle and shell sources. At present, the genetic model of A-type granite mainly includes extensive separation and crystallization of mantle-derived basaltic magma. Assimilative mixing with or without crustal material [52,53]; Re-partial melting of a particular continental crust previously depleted by aqueous felsic melt extraction and possibly mixed with additional new mantle-derived material during melting [33,39,47,51,54–56]. There is a good linear relationship between the major elements of monzonitic granite and granite in Liucun pluton. In Harker's diagram (Figure 5), from monzonitic granite to granite, TiO_2, Al_2O_3, Fe_2O_3, MgO, CaO, P_2O_5 and MnO linearly decrease with the increase of SiO_2 content, while K_2O is positively correlated with SiO_2. It shows typical characteristics of homologous magmatic evolution. In general, the early granite magma is rich in Si and K, while the late monzonitic magma is rich in Fe, Mg and Ca. In the correlation diagrams of La/Sm-La and Rb/Nb-Rb/Zr (Figure 10), the sample values are roughly arranged in oblique lines, showing the trend of partial melting evolution. Therefore, the genesis of Liucun pluton is consistent with the view that the residual refractory material after partial melting is extracted from the melt is partially melted again.

 doi:10.20944/preprints202411.0865.v1

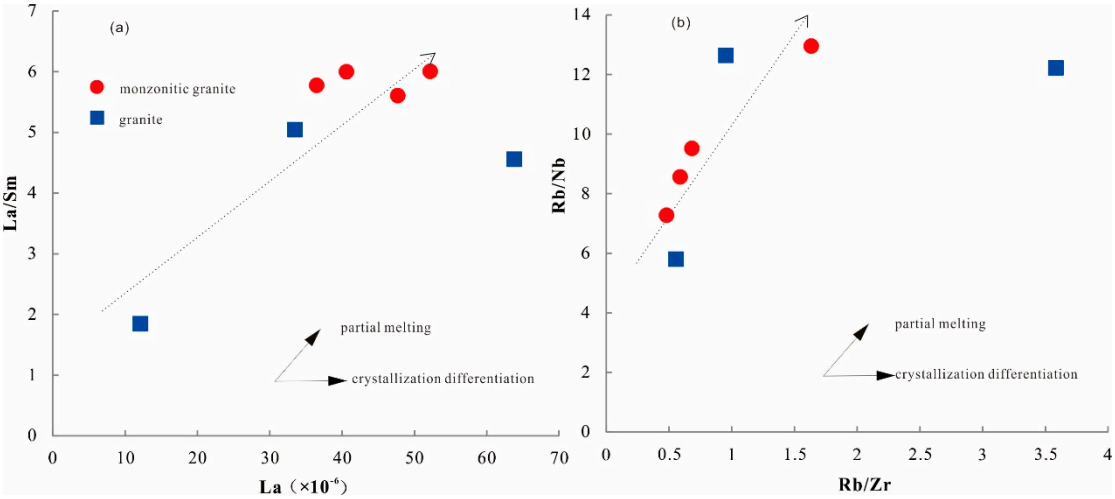

Figure 10. La/Sm vs. La (a) and Rb/Nb vs. Rb/Zr (b) diagrams for the monzonitic granite and granite from Liucun pluton.

The monzonitic granites and granites of the Liucun pluton are rich in SiO_2, poor in MgO, MnO and CaO, with A/CNK close to or greater than 1, rich in light rare earth elements and large ion lithophile elements, and deficient in high field strength elements, and have characteristics similar to island arc magmatic rocks, showing crustal geochemical characteristics [57,58]. The high n (CaO)/[n (MgO) +n (FeO^T)] and low n (Al_2O_3)/[n (MgO) +n (FeO^T)] values also indicate that the primary rocks are mainly derived from partial melting of mafic rocks in the crust [59,60]. Rocks with ε_{Hf} (t) < 0 were formed by partial melting of the ancient lower crust [61,62]. The ε_{Hf} (t) of the Liucun pluton ranges from -10.93 to -6.91, with an average value of -8.50. The two-stage model age (T_{DM2}) of the Liucun pluton ranges from 1658 to 1880Ma. The T_{DM2} of the two-stage model age of the Liucun pluton is mainly 1.7Ga. The second-stage model age of zircon Hf from Mesozoic rocks in the middle and lower reaches of the Yangtze River mainly ranges from 1.0 to 1.5Ga, with a peak age of 1.4Ga [31], which is lower than that of the Liucun pluton. The T-ε_{Hf} (t) diagram of magmatic zircons in the Liucun pluton with ε_{Hf} (t) < 0 shows that the Hf isotope composition of 49 zircons is located near the lower crust evolution curve, between the paleoproterozoic and the depleted mantle evolution line (Figure 11). This indicates that the magma may be formed by partial melting of the ancient lower crust in the mesoproterozoic, which is far from the chondrite evolution line, indicating that the source material of the Liucun pluton is dominated by the ancient lower crust material. The characteristics of major and trace elements and Hf isotopes in Liucun pluton indicate the shell-source characteristics.

However, the Sr, Nd and Hf isotopic compositions of the late Mesozoic intrusive rocks in the eastern section of Jiangnan orogenic belt, including the Liucun pluton, are obviously different from those in the early period, indicating that they have completely different magmatic source regions. There is often a time interval of more than 10Ma between the late Mesozoic A-type granites including Liucun pluton and the early I/S granodiorite emplacement in the eastern section of Jiangnan orogenic belt. The initial values of $^{87}Sr/^{86}Sr$ in the late stage ranged from 0.5780 to 0.7122, mostly concentrated in 0.7072 to 0.7122, while the initial values of $^{87}Sr/^{86}Sr$ in the early stage ranged from 0.6646 to 0.7137, mostly concentrated in 0.7086 to 0.7137. The ε_{Nd} (t) in the late stage ranges from -6.90 to -1.74, mostly concentrated in -6.90 to -4.65, and the peak value is about -6; the εNd (t) in the early stage ranges from -7.68 to -0.54, mostly concentrated in -7.68 to -3.86, and the peak value is about -7. The distribution range of ε_{Nd} (t) value in the late stage is narrower than that in the early stage. The ε_{Hf} (t) in the late stage is also slightly higher than that in the early stage, mainly ranging from -10.93 to -4.63, with a peak value of about -7; the ε_{Hf} (t) in the early stage ranges from -14.20 to -2.46, with a peak value of about -8, and the distribution range of ε_{Hf} (t) values is also narrower than that in the early stage (Figures 12 and 13). In general, the late plutons including the Liucun pluton show a loss and relatively uniform isotopic composition, while the early plutons are enriched with a wide range of variations,

 doi:10.20944/preprints202411.0865.v1

indicating complex shell source composition characteristics. Compared with the early intrusive rocks, the late rocks contain a larger proportion of new mantly-derived materials.

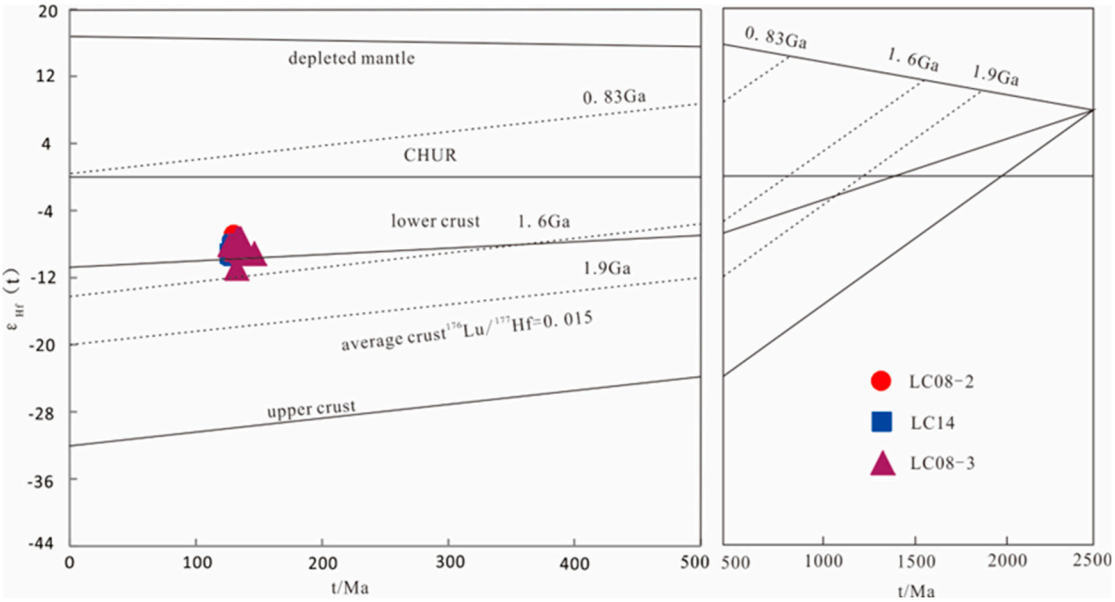

Figure 11. Relationship between ε_{Hf} (t) and age of zircon in Liucun pluton.

The magmatism in the eastern part of Jiangnan uplift zone changed from calc-alkaline I/S-type granites to A-type granites, and ε_{Nd} (t) and ε_{Hf} (t) values became more enriched, indicating that there was an obvious addition of depleted mantle material. In addition, previous studies have shown that A-type granites generally have higher Zr saturation temperature than I/S-type granites, indicating that new mantle source magma from the asthenosphere has been added to the differentiated magma chamber. Moreover, mafic inclusions have been found in some A-type granites, which all indicate the existence of magmatic mixing [38,53]. In summary, we believe that the Liucun pluton is derived from the partial melting of the ancient lower crust again in the Mesoproterozoic, and more new mantle source materials were mixed in the melting process due to the transformation of the tectonic environment.

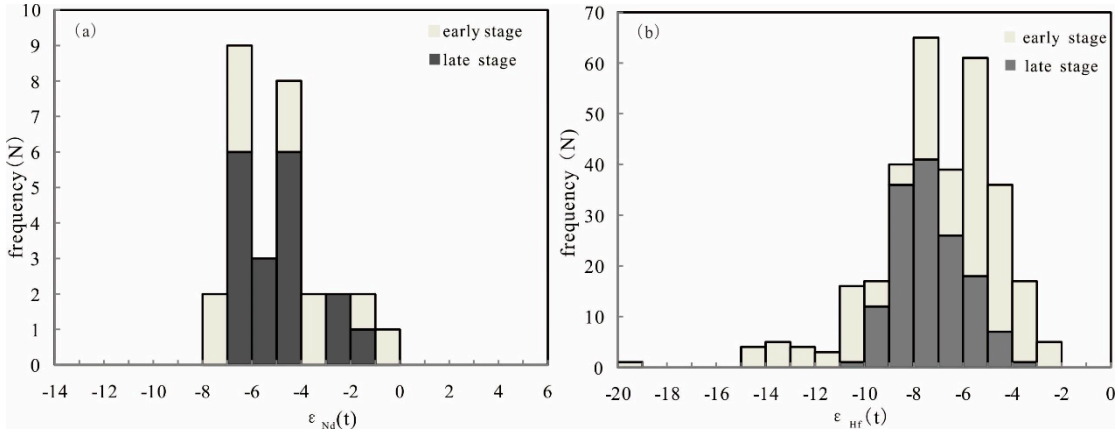

Figure 12. Frequency distribution map of ε_{Nd} (t) and ε_{Hf} (t) values of the Early and Late Mesozoic intrusive rocks in the eastern section of Jiangnan Orogenic Belt (data other than the Liucun pluton from my unpublished data).

 doi:10.20944/preprints202411.0865.v1

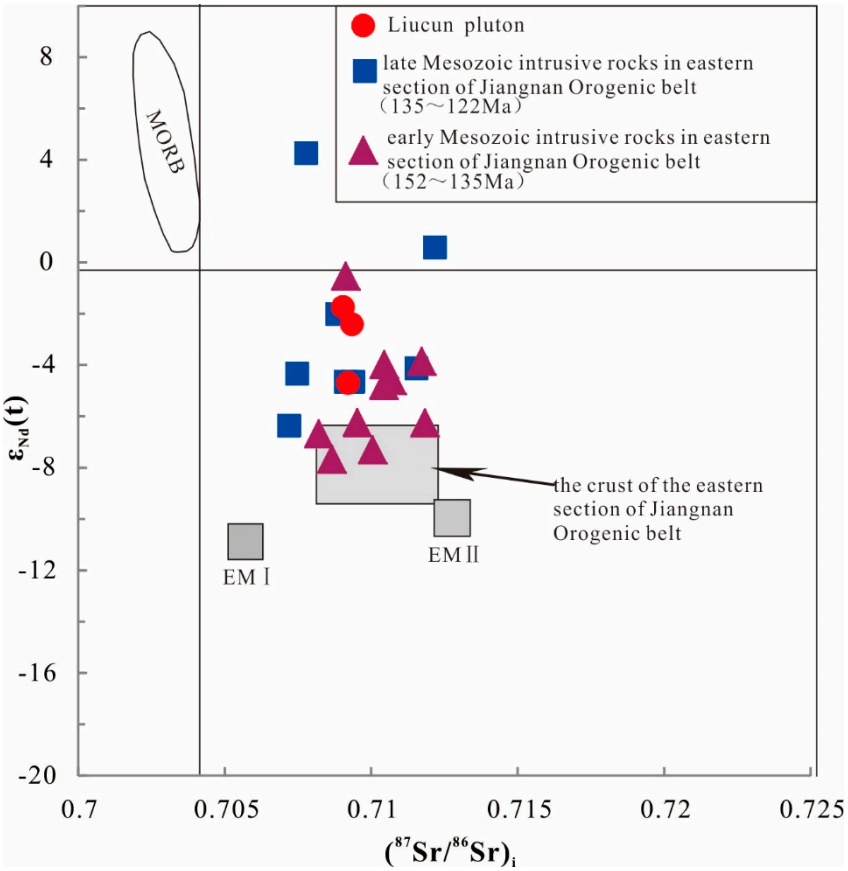

Figure 13. Relationship between εNd（t）and initial 87Sr/86Sr values of Liucun pluton and the Early and Late Mesozoic intrusive rocks in the eastern part of Jiangnan orogenic belt. Data from the papers [5,39,43,46,56,63],including this paper and my unpublished data;.

With frequent tectonic movement and magmatic activity, southeast China is one of the regions with the most complex structure and evolution in the global continental lithosphere, as well as one of the most significant research areas in the global continental lithosphere [18]. The study area has experienced many orogeny since the Middle Proterozoic. In Neoproterozoic, the collision between the Yangtze block and the South China block formed the Jiangnan orogenic belt [64,65]. The Indochin-Yanshan movement triggered strong magmatic activity in this zone, and formed the late Mesozoic intrusions that are currently distributed in bands. As for the dynamic mechanism of late Mesozoic magmatism in the region, most scholars believe that it is closely related to the subduction of the Paleo-Pacific plate to Eurasia and the subsequent recessional of the subduction plate, and is also the key to the late Mesozoic mineralization in South China [18,39,66]. Under the influence of the subduction of the Paleo-Pacific plate, the whole South China underwent a dynamic regime transformation at the turn of the late Jurassic-early Cretaceous, and the tectonic environment changed from compressive to tensile [39,67–70].

According to the Y-Nb tectonic environment discriminant map of Liucun pluton, monzonitic granite falls near the dividing line of volcanic arc granite, synclastic granite and intraplate granite, and the granite falls within the intraplate granite region (Figure 14a). According to the Yb-Ta tectonic environment discriminant map, the monzonitic granite mainly falls in the volcanic arc granite, and the granite is all in the intra-plate granite region (Figure 14b). In the Sr/Y-Y diagram, monzonitic granite and granite all fall into the classical island arc rocks (Figure 14c). In the Y+Nb-Rb diagram, the monzonitic granite falls into the volcanic arc granite zone, and the granite falls into the intra-plate granite and the boundary line with the volcanic arc granite, and all fall into the post-collision granite (Figure 14d). This indicates that the formation of the main body of the Liucun pluton (monzonitic granite) may be affected by collision, and the pluton was formed in post-collision or post-collision

 doi:10.20944/preprints202411.0865.v1

intraplate tensile environment, which is consistent with previous research results on A-type granite in southern Anhui province [18,33,38,39,71,72].

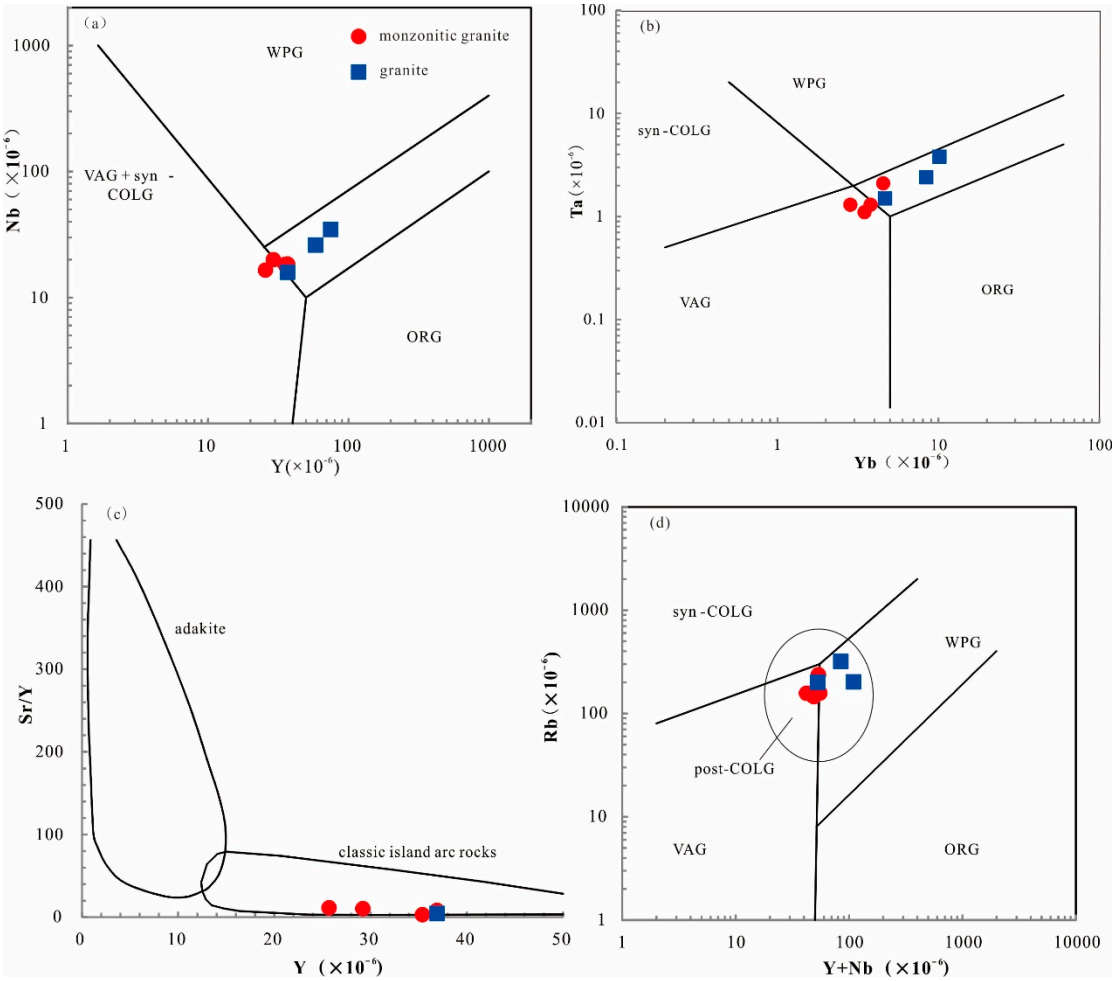

Figure 14. Discriminant diagram of tectonic background of Liucun pluton (a, b, d after the paper [57]; c after the paper [58]) WPG- withinplate granite; Vag-volcanic arc granite; syn-COLG- syncollisional granite; ORG- mid-ocean ridge plagioclase granite; post-COLG–post-collisional granite.

The formation of I/S-type granites in the eastern section of the Jiangnan uplift belt in the late Mesozoic and early stages may be related to the retraction of the Pacific plate after flat subduction [44,73], at this time, the whole South China was in a compressive environment in the late Jurassic, which lasted until the early Cretaceous, and the plate movement at this time also caused a small amount of mantle-derived magma to invade the old and thickened lower crust, forming I/S-type granite. Later A-type granites may be formed in the beginning stage of intraplate stretching or continental rift, under the tectonic background of stress relaxation after extrusion to continuous tensile extension [56]. The crust and lithospheric mantle gradually became thin, and the asthenosphere continuously upflowed. The partial melting of the crustal base metamorphic basalt and lower crustal metamorphic sedimentary rock (or metamorphic igneous rock) mixed bodies, which were thickened by introntinental orogeny in the late Triassic and early Jurassic, was triggered successively [39]. From the late Jurassic to early Cretaceous, with the increase of plate subduction angle, the intraplate stretching effect gradually increased. Asthenosphere upsurge led to the melting of the subcontinental lithosphere mantle, resulting in a large number of new basaltic magma. With the floor encroaching of these new mantly-derived materials, the mesoproterozoic basement rocks were melted on a large scale, so the A-type granites were produced. At the same time, one stage mineralization also developed in this magmatism, which is similar to the mineralization of double peak type magmatic rocks in the middle and lower reaches of the Yangtze River metallogenic belt

[72], and is also represented by numerous copper polymetallic deposits (points) around the Liucun pluton.

6. Conclusions

The LA-ICP-MS U-Pb weighted mean ages of zircon La-ICP-MS U-Pb from monzonitic granite and porphyritic biotite monzonitic granite in Liucun pluton are 130.50±0.55Ma and 128.95±0.46Ma respectively. The LA-ICP-MS U-Pb weighted mean age of zircon from the granite is 133.8±1.0Ma. It is the product of magmatic activity in the late stage of Jiangnan uplift belt, and the emplacement time of granite is slightly earlier than that of monzonitic granite.

The occurrence characteristics of rare earth elements in the weathering crust of Liucun pluton are worthy of further study. The characteristics of major, trace and rare earth elements in the Liucun pluton are typical A-type granites. Meanwhile, the characteristics of major, trace elements and Hf isotopes indicate the shell source characteristics of the Liucun pluton. The $(^{87}Sr/^{86}Sr)_i$ value of the late Mesozoic intrusive rocks in the eastern part of Jiangnan orogenic belt, including the Liucun pluton, is smaller than that in the early stage, and the ε_{Nd} (t) and ε_{Hf} (t) values in the late stage are larger than that in the early stage, and the distribution range is narrower than that in the early stage. The Liucun pluton is derived from the secondary partial melting of the ancient lower crust in Mesoproterozoic, and during the melting process, more new mantle source materials were mixed in due to the transformation of tectonic environment.

The main body of the Liucun pluton, the monzonitic granite, has the characteristics of volcanic arc and classical island arc rocks, indicating that the formation of the main body of the pluton was influenced by collision, and the pluton was formed in the intraplate stretching environment after the tectonic transition period from the late Jurassic to the early Cretaceous, and one stage mineralization was also developed in the magmatism during this period, which is manifested by numerous copper polymetallic deposits (points) around the Liucun pluton.

References

1. Ding N, Chen F, Tang C. Yanshanian metallogenic characteristics and metallogenic specificity of magmatic rocks in southern Anhui. Geology of Anhui, 2023, 33(3):193-197.
2. Zheng W, Chen TH, Du JG, Chen F, Ding N, Zhang S. Petrogenesis of Fuling A- type granite in southern Anhui : Geochemistry, Zircon U-Pb age and Lu-Hf isotope characteristics.Geological Review,2024,70(1):189-206.
3. Zhou TF, Yuan F,Hou MJ, Du JG, Fan Y, Zhu G and Yue SC. Comparative study of metallogenic conditions and resource potential in the eastern section of Jiangnan uplift in Anhui and Jiangxi adjacent areas. Progress in Natural Science, 2003,13(10): 1036-1041 .
4. Zhou TF,Yuan F,Hou MJ,Du JG, Fan Y, Zhu G and Yue SC. Genetic and dynamic background of Yanshanian granitoids in Anhui-Jiangxi adjacent area, eastern Jiangnan orogenic belt. Journal of Mineralogy and Petrology. 2004,24(3):65-71.
5. Zhou J, Jiang YH and Ge WY. High Sr/Y Jingde pluton in the Eastern Jiangnan Orogen, South China: formation mechanism and tectonic implications.Acta Geologica Sinica, 2014, 88(1)53-62.
6. Zhou SZ, Xu SF, Yu XQ, Qiu JT, Yang XP, Chen ZW and Liu X. Zircon LA-ICP-MS U-Pb ages and geochemical features of Taiping pluton in South Anhui—Enlightment of Mesozoic lithospheric thinning for South China. Geological Review, 2016,62(6):1549-1564.
7. Chen RL, Pan JY, Wu JJ and Chen F. Study of Zircon U-Pb age and characteristics of Hf isotopes of the Maolin granodiorite in Jiangxi County, southern Anhui Province. Geological Bulletin of China, 2019,38(7):1219-1227.
8. Li PJ, Yu XQ, Qiu JT, Li HY, Chen ZW and Han YC. Petrogenesis, oxygen fugacity characteristics and mineralization significance of two kinds of Jurassic-Cretaceous granites in southern Anhui, SE China. Acta Petrologica Sinica, 2016,32(2) : 399-418.
9. Mao JW, Xiong BK, Liu J, Pirajno F, Cheng YB, Ye HS, Song SW and Dai P. Molybdenite Re/Os dating, zircon U-Pb age and geochemistry of granitoids in the Yangchuling porphyry W-Mo deposit(Jiangnan tungsten ore belt) , China: Implications for petrogenesis, mineralization and geodynamic setting. Lithos, 2017, 286- 287:35-52.
10. Jiang SY, Peng NJ, Huang LC, Xu YM, Zhan GL and Dan XH. Geological characteristic and ore genesis of the giant tungsten deposits from the Dahutang ore-concentrated district in northern Jiangxi Province. Acta Petrologica Sinica, 2015,31 (3): 639-655.

11. Chen F, Wang DH, Du JG, Xu W, Wang KY, Yu YL and Tang JL. Geochemical Characteristics and LA-ICP-MS Zircon U-Pb Age of the Lanhualing Granite in Ningguo, Anhui Province.Geotectonica et Metallogenia, 2015,39(2):369-377.
12. Li B, Zhang ZZ, Wu MA, Zhou TF, Zhao WG, Cai XB and Di QS. LA-ICP-MS zircon U-Pb age and molybdenite Re-Os dating of the Dawujian W-Mo polymetallic deposit, Ningguo, Anhui Province.Geological Bulletin of China, 2015,34(2 -3) :569–578.
13. Kong ZG, Liang T, Mao JW, Xu SF, Xu HB, Yan PP, and Jin XY. Study on perogenesis of granodiorite, metallogenic epoch and petrogenetic-metallogenetic setting in the Zhuxiling tungsten polymetallic deposit, southern Anhui Province, China. Acta Petrologica Sinica, 2018,34(9):2632-2656
14. Hou SY, Zhang DY, Zhang F, Lei XX, Hu MX,Weng WF,Noel CW. Geochronology, geochemical characteristics , and mineralization significance of the granodiorite porphyry in Sanbao lead-zinc deposit,eastern Jiangnan orogenci belt. Geotectonica et Metallogenia,2024,48(4):879-898.
15. Chen F, Wang DH, Du JG, Xu W, Hu HF,Wang KY,Yu YL and Tang JL. Geochemical characteristics and LA-ICP-MS zircon U-Pb geochronology of the Liucun monzogranite in Ningguo, Anhui Province and their geological significance. Acta Geologica Sinica, 2014, 88(5):869-882.
16. Wu JF, Lu XS, Chu DR. Geochemical features, zircon U-Pb dating and genetic study of the Liucun rockmass in Guangde County, Anhui. Geology of Anhui, 2017,27(3):161-167.
17. Liu GS. Deformation characteristics and evolution of the Jiangnan fault zone（segment of southern Anhui ）since Sinian Period. Journal of Hefei University of Technology（Natural Science）, 1997,20（3）: 97-102.
18. Xie JC, Xia DM, Fang D, Yan J, Yang XY, Sun WD and Li QZ. Geochemistry of Late Mesozioc granodiorites in southern Anhui Province : Constraints for rock-and ore-forming. Acta Petrologica Sinica , 2016,32（02）: 439-455.
19. Zhang G, Ren SL, Chen GT, Li LM, Song CZ, Li JH, Lin SF and Li ZQ. Geochronology, geochemistry and tectonic significance of Houshan and Maolin pluton in the Jiangnan uplift belt. Chinese Journal of Geology, 2021,56(3):884-913.
20. Yu XQ, Jiang LL, Xu W, Qiu RL, Du JG and Dai SQ. Identification and basic characteristics of the Anhui-Zhejiang-Jiangxi fault zone. Earth Science Frontiers, 2007,14(3):102-113.
21. Zhou SZ, Xu SF, Yu XQ, Qiu JT, Yang XP, Chen ZW and Liu X. Zircon LA-ICP-MS U-Pb ages and geochemical features of Taiping pluton in South Anhui—Enlightment of Mesozoic lithospheric thinning for South China. Geological Review, 2016,62(6):1549-1564.
22. Wang XL, Zhou JC, Griffin WL, Zhao GC, Yu JH, Qiu JS, Zhang YJ and Xing GF. Geochemical zonation across a Neoproterozoic orogenic belt: Isotopic evidence from granitoids and metasedimentary rocks of the Jiangnan orogen, China. Precambrian Research, 2014, 242:154-171.
23. Li LY, Han Y, Zhang CH. Geochronology, geochemical characteristics and geological significance of Jingtan Formation in Anhui Province.Geological Review, 2024,70(Supp.1):191-192.
24. Xue HM, Ma F, Song YQ and Xie YP. Geochronology and geochemisty of the Neoproterozoic granitoid association from eastern segment of the Jiangnan orogen, China: Constraints on the timing and process of amalgamation between the Yangtze and Cathaysia blocks. Acta Petrologica Sinica, 2010,26(11) : 3215-3244.
25. Xie JC, Chen S, Rong W, Li QZ, Yang XY and Sun WD. Geochronology, geochemistry and tectonic significance of Gunujiang A-type granite in Anhui Province. Acta Petrologica Sinica, 2012,28(12) :4007 -4020.
26. Wilson M. Igneous petrogenesis: aglobal tectonic approach. London: Unwin Hyman, 1989,1-466.
27. Sun SS and Mc Donough WF. Chemical and isotopic systematics of oceanic basalts: Implications for mantle composition and processes. In: Saunders AD and Norry MJ (eds.) . Magmatism in the Ocean Basins. Geological Society, London, Special Publication, 1989,42 (1):313-345.
28. Gao L, Yan J, Li QZ, Xie JC. Occurrence characteristics of REE in granite weathering crust of Yaocun granite in southern Anhui.Geological Review, 2022,68(5):1820-1838.
29. DePaolo,D.J.. Trace element and isotopic effects of combined wallrock assimilation and fractional crystallization. Earth and Planwtary Science Letters ,1981,53,189-202.
30. Li XH, Zheng YF and Gao S. Lu-Hf isotopic systematics and their applications in petrology. Acta Petrologica Sinica, 2007,23（2）:185-220.
31. Wu FY, Ji WQ, Sun DH, Yang YH and Li XH. Zircon U-Pb geochronology and Hf isotopic compositions of the Mesozoic granites in southern Anhui Province, China. Lithos, 2012, 150: 6 -25.
32. Fu X, Zhang DY, Jiang H, Ye LX, Ren KD, Wang YG, Yuan F and Zhou TF. Genesis of the Xianxia batholith in the Jiangnan Orogenic Belt and its geological significance. Geotectonica et Metallogenia,2020,44(3):543-560.
33. Wang CZ, Huang ZZ, Zhao XL, Chu PL, Huang WC, Song SM, Xu Y, Yang C. Geochronology, geochemistry and petrogenesis of early Cretaceous Yaocun A-type granite in the Lower Yangtze region.Geology in China. 2021,48(2):549-563.

34. He M, Wang X, Deng JL, Wu JF, Wu H and Wu H. Zircon U-Pb geochronology and petrogeochemistry of the Miaoxi plutons in the Guangde area,Anhui Province.Geology of Anhui, 2021,31(3):193-224.
35. Song GX, Qin KZ, Li GM, Noreen JE, and Li XH. Mesozoic Magmatism and Metallogeny in the Chizhou Area, Middle-Lower Yangtze Valley, SE China: Constrained by Petrochemistry, Geochemistry and Geochronology. Journal of Asian Earth Sciences, 2014, 91, 137-153.
36. Yan J，Hou TJ，Wang AG，Wang DE，Zhang DY，Weng WF，Liu JM，Liu XQ and Li QZ. Petrogenetic contrastive studies on the Mesozoic early stage ore-bearing and late stage ore-barren granites from the southern Anhui Province. Science China (Earth Sciences) ，2017,47（11）：1920-1941.
37. Wang CZ, Zhu QB,Jin GD, Chu PL, Liu K. Discussion on the evolution of the Southern Anhui Plateau: Evidence from the Yanshanian two-stage granite in the southern Anhui Province and its adjacent area. Geological Bulletin of China, 2024， 42(2/3):390-400.
38. Xue HM，Wang YG，Ma F，Wang C，Wan DE and Zuo YL. Zircon U-Pb SHRIMP ages of the Taiping (calc-alkaline) -Huangshan (alkaline) composite intrusion: Constraints on Mesozoic lithospheric thinning of the southeastern Yangtze Craton，China. Science in China (Series D) ，2009，52: 1756-1170.
39. Xue HM. Geochronology,geochemistry and stratospheric interactions of Late Mesozoic granitoids near the boundary between Anhui and Zhejiang provinces in the eastern segment of the Jiangnan orogenic belt. Acta Petrologica Sinica, 2021，37(2):433-461.
40. Qin Y，Wang DH，Wu LB，Wang KY and Mei YP. Zircon SHRIMP U-Pb dating of the mineralized porphyry in the Dongyuan W deposit in Anhui Province and its geological significance. Acta Geologica Sinica，2010，84（4）：479-484.
41. Zhou X，Yu XQ，Wang DE，Zhang DH，Li CL，Fu JZ and Dong HM. Characteristics and geochronology of the W，Mo-bearing granodiorite porphyry in Dongyuan，southern Anhui. Geoscience ，2011，25(2) : 201–210.
42. Zhang JJ，Wang GJ，Yang XY，Sun WD and Dai SQ. The petrogenesis of the Jingde granodiorite and its MMEs: Constraints from geochemistry，zircon U-Pb dating and Hf isotopic compositions. Acta Petrologica Sinica，2012,28 (12) : 4047-4063.
43. Su YP，Zheng JP，Griffin WL，Zhao JH，O′ Reilly S Y，Tang HY，Ping XQ and Xiong Q. Petrogenesis and geochronology of Cretaceous adakitic，I- and A-type granitoids in the NE Yangtze Block: Constraints on the eastern subsurface boundary between the North and South China blocks. Lithos，2013,175/176: 333-350.
44. Zhu HL，Yang XY and Sun WD. The petrogenesis of granodiorite in Sanbao area，Qimen County，southern Anhui: Constraints from geochemistry，zircon U-Pb dating and Hf isotope. Acta Petrologica Sinica，2015,31（7）: 1917-1928.
45. Gao R, Yan J, Li QZ, Liu XQ, Wang SN. Petrogenesis of Tanshan pluton in the southern Anhui Province: chronological and geochemical constraints. Geological Journal of China Universities, 2017,23(2):227-243.
46. Yue Q，Yan J，Liu JM，Xie JC，Li QZ and Luo QK. Geochronology，petrogenesis and tectonic implications of the Early Cretaceous granitoids in the Jingde-Guangde area，Anhui Province，South China. Journal of Asian Earth Sciences，2020,190: 104-150.
47. Whalen JB，Currie KL and Chappell BW. A-type granites:Geochemical characteristics，discrimination and petrogenesis. Contributions to Mineralogy and Petrology, 1987,95: 407-419.
48. Bonin B. A-type granites and related rocks: Evolution of a concept, problems and prospects. Lithos, 2007, 97: 1-29.
49. Loiselle MC, Wones DR. Characteristics of anorogenic granites. Geological Society of America Abstracts with Programs, 1979,11(7):468.
50. Frost BR, Frost CD. A geochemical classification for feldspathic igneous rocks. Journal of Petrology, 2008,49:1955-1969.
51. Collins WJ, Beams SD, White AJR, Chappell BW. Nature and origin of A-type granites with particular reference to southeastern Australia. Contributions to Mineralogy and Petrology, 1982,80:189-200.
52. Anderson IC，Frost CD and Frost BR. Petrogenesis of the Red Mountain pluton，Laramie anorthosite complex，Wyoming:Implications for the origin of A-type granite. Precambrian Research，2003,124: 243-267.
53. Wong J，Sun M，Xing GF，Li XH，Zhao GC，Wong K，Yuan C，Xia XP，Li LM and Wu FY. Geochemical and zircon U-Pb and Hf isotopic study of the Baijuhuajian metaluminous A-type granite:Extension at 125～100Ma and its tectonic significance for South China. Lithos, 2009,112: 289-305.
54. Creaser RA，Price RC and Wormald RJ. A-type granites revisited:Assessment of a residual source model. Geology，1991,19: 163-166.
55. Jiang YH，Zhao P，Zhou Q，Liao SY and Jin GD. Petrogenesis and tectonic implications of Early Cretaceous S-and A-type granites in the northwest of the Gan-Hang rift，SE China. Lithos，2011,121: 55-73.

56. Yang SY，Jiang SY，Zhao KD，Jiang YH，Ling HF and Luo L. Geochronology，geochemistry and tectonic significance of two Early Cretaceous A-type granites in the Gan-Hang Belt，Southeast China. Lithos, 2012,150: 155-170.
57. Pearce JA, Harris NBW and Tindle AG. Trace element discrimination diagrams for the tectonic interpretation of granitic rocks. Journal of Petrology，1984,25: 956-983.
58. Defant MJ and Kepezhinskas P. Evidence suggests slab melting in arc magmas. EOS(Transactions, American Geophysical Union), 2001, 82(6) : 65-69.
59. Altherr R, Holl A, Hegner E, Langer C, Kreuzer H. High-potassium, calcalkaline I- type plutonism in the European Variscides, northern Vosges (France) and northern Schwarzwald(Germany). Lithos, 2000,50: 51-73.
60. Wang YJ, Fan WM, Guo F, Peng TP, Li CW. 2003. Geochemistry of Mesozoic mafic rocks adjacent to the Chenzhou Linwu fault, South China:Implications for the lithospheric boundary between the Yangtze and Cathaysia blocks. International Geology Review, 45(3): 263-286.
61. Vervoort JD, Patchett PJ, Blichert-Toft J, Albarède F. Relationships between Lu-Hf and Sm-Nd isotopic systems in the global sedimentary system.Earth and Planetary Science Letters, 1999,168(1- 2) :79-9.
62. Griffin W L, Wang X, Jackson S E, Pearson N J,O′ Reilly S Y, Xu X S, Zhou X M.Zircon chemistry and magma mixing, SE China: In-situ analysis of Hf isotopes, Tonglu and Pingtan igneous complexes. Lithos, 2002,61(3-4) : 237-269.
63. Zhou X，Yu XQ，Wang DE，Zhang DH，Li CL，Fu JZ and Dong HM. Characteristics and geochronology of the W，Mo-bearing granodiorite porphyry in Dongyuan，southern Anhui. Geoscience ，2011,25(2) : 201–210.
64. Guo LZ，Lu HF，Shi YS，Ma RS，Sun Y，Shu LS，Jia D，Zhang QL，Charvet J and Faure M. On the Meso-Neoproterozoic Jiangnan island arc: Its kinematics and dynamics．Geological Journal of China Universities，1996,2(1) : 1-13.
65. Zhu G and Liu GS. Basic characteristics and mesozoic orogenic process of the Jiangnan intracontinental orogenic belt in Southern Anhui. Geotectonica et Metallogenia, 2000,24 (2) :103-111.
66. Wang FY，Ling MX，Ding X，Hu YH，Zhou JB，Yang XY，Liang HY，Fan WM and Sun WD．Mesozoic large magmatic events and mineralization in SE China: Oblique subduction of the Pacific plate．International Geology Review，2011,53(5 -6) : 704-726.
67. Holloway NH. North Palawan Block, Pliilippines——its relation to Asian Mainl and role in evolution of South China Sea. The American Association of Petroleum Geologists Bulletin, 1982,66(9):1355-1383.
68. Charvet, J., Lapierre, H., and Yu, Y. W. Geodynamic significance of the Mesozoic volcanism of southeastern China. J. Southeast Asian Earth Sci. 1994,9: 387–396.
69. Shu LS, and Zhou XM. Late Mesozoic tectonism in Southeast China. Geological Review, 2002,48(3):249-260.
70. Yu XQ, Wu GG, Zhang D, Di YJ, Zang WS, Zhang XX, and Wang QF. The research progress of the Mesozoic tectonic regime transition in southeastern China. Progress in Natural Science, 2005,15(10):1167-1175.
71. Zhang S，Zhang ZC，Ai Y，Yuan WM and Ma LT. The petrology，mineralogy and geochemistry study of the Huangshan granite intrusion in Anhui Province. Acta Petrologica Sinica，2009, 25 (1) : 25-38.
72. Bai RY, Xu XC, Du JG, Dai SQ, Zhang DY, and Che YD. Characteristics and U-Pb dating of zircons for intermediate-acidic dikes inQingyang-Jingxian area of South Anhui Province and their geological significance. Mineral Deposits, 2019,38(2):401-425.
73. Chen XF，Wang YG，Sun WD and Yang XY. Zircon U-Pb chronology，geochemistry and genesis of the Zhuxiling granite in Ningguo，southern Anhui. Acta Geologica Sinica，2013,87（11）: 1662 -1678.